ELEMENTA
Science of the Anthropocene

Fe availability drives phytoplankton photosynthesis rates during spring bloom in the Amundsen Sea Polynya, Antarctica

Anne-Carlijn Alderkamp[1*] • Gert L. van Dijken[1] • Kate E. Lowry[1] • Tara L. Connelly[2,6] • Maria Lagerström[3,7] • Robert M. Sherrell[3,4] • Christina Haskins[3] • Emily Rogalsky[3] • Oscar Schofield[3] • Sharon E. Stammerjohn[5] • Patricia L. Yager[2] • Kevin R. Arrigo[1]

[1]Department of Environmental Earth System Science, Stanford University, Stanford, California, United States
[2]Department of Marine Sciences, University of Georgia, Athens, Georgia, United States
[3]Department of Marine and Coastal Sciences, Rutgers University, New Brunswick, New Jersey, United States
[4]Department of Earth and Planetary Sciences, Rutgers University, New Brunswick, New Jersey, United States
[5]Institute of Arctic and Alpine Research, University of Colorado, Boulder, Colorado, United States
[6]Marine Science Institute, The University of Texas at Austin, Port Aransas, Texas, United States
[7]Department of Applied Environmental Science (ITM), Stockholm University, Stockholm, Sweden
*alderkamp@stanford.edu

Abstract

To evaluate what drives phytoplankton photosynthesis rates in the Amundsen Sea Polynya (ASP), Antarctica, during the spring bloom, we studied phytoplankton biomass, photosynthesis rates, and water column productivity during a bloom of *Phaeocystis antarctica* (Haptophyceae) and tested effects of iron (Fe) and light availability on these parameters in bioassay experiments in deck incubators. Phytoplankton biomass and productivity were highest (20 µg chlorophyll *a* L^{-1} and 6.5 g C m^{-2} d^{-1}) in the central ASP where sea ice melt water and surface warming enhanced stratification, reducing mixed layer depth and increasing light availability. In contrast, maximum photosynthesis rate (P^*_{max}), initial light-limited slope of the photosynthesis–irradiance curve (α^*), and maximum photochemical efficiency of photosystem II (F_v / F_m) were highest in the southern ASP near the potential Fe sources of the Dotson and Getz ice shelves. In the central ASP, P^*_{max}, α^*, and F_v / F_m were all lower. Fe addition increased phytoplankton growth rates in three of twelve incubations, and at a significant level when all experiments were analyzed together, indicating Fe availability may be rate-limiting for phytoplankton growth in several regions of the ASP early in the season during build-up of the spring bloom. Moreover, Fe addition increased P^*_{max}, α^*, and F_v / F_m in almost all experiments when compared to unamended controls. Incubation under high light also increased P^*_{max}, but decreased F_v / F_m and α^* when compared to low light incubation. These results indicate that the lower values for P^*_{max}, α^*, and F_v / F_m in the central ASP, compared to regions close to the ice shelves, are constrained by lower Fe availability rather than light availability. Our study suggests that higher Fe availability (e.g., from higher melt rates of ice shelves) would increase photosynthesis rates in the central ASP and potentially increase water column productivity 1.7-fold, making the ASP even more productive than it is today.

Domain Editor-in-Chief
Jody W. Deming, University of Washington

Associate Editor
Jean-Éric Tremblay, Université Laval

Knowledge Domain
Ocean Science

Article Type
Research Article

Part of an *Elementa* Special Feature
ASPIRE: The Amundsen Sea Polynya International Research Expedition

Received: May 20, 2014
Accepted: March 01, 2015
Published: April 8, 2015

Introduction

Antarctic shelf waters are strong sinks for atmospheric CO_2 due to high biological productivity, intense winds, high air-sea gas exchange, formation of bottom water and extensive winter ice cover. These factors make these regions important for the biogeochemical cycling of elements, particularly of carbon (C) (Sarmiento et al., 2004; Arrigo et al., 2008). Specifically, coastal polynyas (areas of open water surrounded by ice) are hot spots for energy and C transfer between the atmosphere and ocean (Smith and Barber, 2007, Mu et al., 2014). The reduced ice cover increases air-sea gas exchange and results in enhanced light availability in the water column

in early spring, thereby increasing primary productivity through phytoplankton photosynthesis. In addition to its importance for the global C cycle, phytoplankton productivity supports the biota occupying higher trophic levels including krill, penguins, and whales (Arrigo et al., 2003; Ainley et al., 2006).

Phytoplankton productivity in the Southern Ocean is often limited by the availability of iron (Fe) (Boyd et al., 2007, and references therein), although light limitation may also occur due to deep vertical mixing below the critical depth (Mitchell et al., 1991; De Baar et al., 2005). The Fe supply for phytoplankton growth in polynyas is enhanced compared to the open ocean due to input of dissolved Fe (DFe) from melting sea ice (Sedwick and DiTullio, 1997; Lannuzel et al., 2010), shelf sediments (Hatta et al., 2013; De Jong et al., 2013), icebergs (Raiswell et al., 2008; Raiswell, 2011; Shaw et al., 2011), upwelling Circumpolar Deep Water (CDW) (Klunder et al., 2011), remineralized Fe in winter water (WW), and melting glaciers (Raiswell et al., 2006; Gerringa et al., 2012, Sherrell et al., 2015). Despite these sources, phytoplankton growth is often still seasonally Fe-limited in later stages of blooms in polynyas such as in the Ross Sea Polynya (Sedwick and DiTullio, 1997; Sedwick et al., 2000; Tagliabue and Arrigo, 2005) and the Weddell Sea (Buma et al., 1991). Bioassay experiments in the Ross Sea Polynya revealed that phytoplankton growth was Fe-limited later in the season, but not early (Sedwick and DiTullio, 1997; Sedwick et al., 2000). It is believed that phytoplankton blooms gradually draw down a "winter stock" of DFe in the WW that eventually limits the bloom, especially away from DFe sources such as sea ice (Hopkinson et al., 2013). However, recent measurements show low and potentially limiting concentrations of DFe early in the season (Sedwick et al., 2011; Marsay et al 2014), implying that significant sources of new DFe are required to sustain a phytoplankton bloom throughout the season.

Satellite estimates of primary productivity in Antarctic polynyas reveal the highest productivity per surface area in the Amundsen Sea (Arrigo and Van Dijken, 2003). The Amundsen Sea contains two polynyas, the Pine Island Polynya (PIP) in the east and the Amundsen Sea Polynya (ASP) in the west. The Amundsen Sea is located in the western Antarctic, where rates of ice sheet thinning are the highest in all of Antarctica (Pritchard et al., 2009; Rignot et al., 2013). Several fast-flowing glaciers that are rapidly thinning drain into the Amundsen Sea where they form floating ice shelves or glacier tongues that are also thinning (Randall-Goodwin et al., 2015). These are the Pine Island Glacier in the PIP and the Getz and Dotson glaciers in the ASP. The Thwaites and Crosson glaciers form ice tongues between the PIP and ASP and may affect both polynyas (Pritchard et al., 2009; Rignot et al., 2013).

The thinning of the ice shelves is mainly attributed to regional bathymetry and oceanography. As the Antarctic Circumpolar Current (ACC) flows close to the continental shelf break, Circumpolar Deep Water (CDW) intrudes southward through deep troughs onto the Antarctic continental shelf (Jacobs et al., 1996, 2011; Arneborg et al., 2012). On the shelf, the CDW mixes with WW and becomes modified CDW (mCDW) that is warm (> 0.6°C) and salty (> 34.5) relative to WW. Near the coast, mCDW has access to ice shelf cavities and drives basal melting of floating ice shelves (Jenkins et al., 2010; Jacobs et al., 2011, 2013; Dutrieux et al., 2014). The resulting mCDW mixed with glacial melt water (meltwater-laden mCDW) becomes fresher (< 34.0), colder (–1.1 to –0.5°C), and more buoyant. At the surface of the ASP, Antarctic Surface Water (AASW) shows a range in salinity (33.6 to 34.1) and temperature (–1.8 to > 0°C), depending on length of time since sea ice melt, degree of solar warming, and wind- or buoyancy-induced mixing with the underlying waters (Yager et al., 2012; Ha et al., 2014). The meltwater-laden mCDW outflowing at subsurface depths from under the Dotson ice shelf (DIS) appears to be a major source of DFe and Particulate Fe (PFe) to the phytoplankton bloom in the ASP (Gerringa et al., 2012; Sherrell et al., 2015). This subsurface source is likely made available to AASW at the surface through horizontal diffusivity (Gerringa et al., 2012), advective eddy transport (e.g., Årthun et al., 2013), mixing along the Dotson trough (e.g., St-Laurent et al., 2013), and by wind- and iceberg-induced mixing (Randall-Goodwin et al., 2015). Similarly, the meltwater-laden mCDW from the Pine Island Glacier was found to be a major source of DFe for the phytoplankton bloom in the PIP (Gerringa et al., 2012). These Fe sources support phytoplankton blooms with high biomass and productivity in both the PIP and ASP (Alderkamp et al., 2012a; Yager et al., 2012). Moreover, Fe addition bioassay experiments at the peak and during the decline of the phytoplankton bloom revealed that Fe was not limiting phytoplankton growth in either polynya at these times (Mills et al., 2012), suggesting relatively high Fe availability to the phytoplankton.

Light availability for phytoplankton in Antarctic polynyas is temporally and spatially variable. Early in the season, the shrinking sea ice cover, in combination with increasing day length and solar elevation, results in greater light availability in surface waters. After the polynya opens up, light availability is determined by cloud cover, mixed layer depth (MLD), and attenuation in the water column that is controlled primarily by phytoplankton biomass. In general, melting sea ice introduces fresh water at the surface, which stabilizes the water column and creates a well-lit shallow mixed layer. Conversely, basal ice shelf melt introduces meltwater-laden mCDW into the water column at the base of the ice shelf, at 150-400 m depth, depending both on the draft of the ice shelf (Jacobs et al., 2012; Mankoff et al., 2012) and the degree of buoyancy driven upwelling. Introducing buoyant water at depth destabilizes the water column and may increase MLD and decrease light availability to the phytoplankton, as was observed at the face of the Pine Island ice shelf (Alderkamp et al., 2012a).

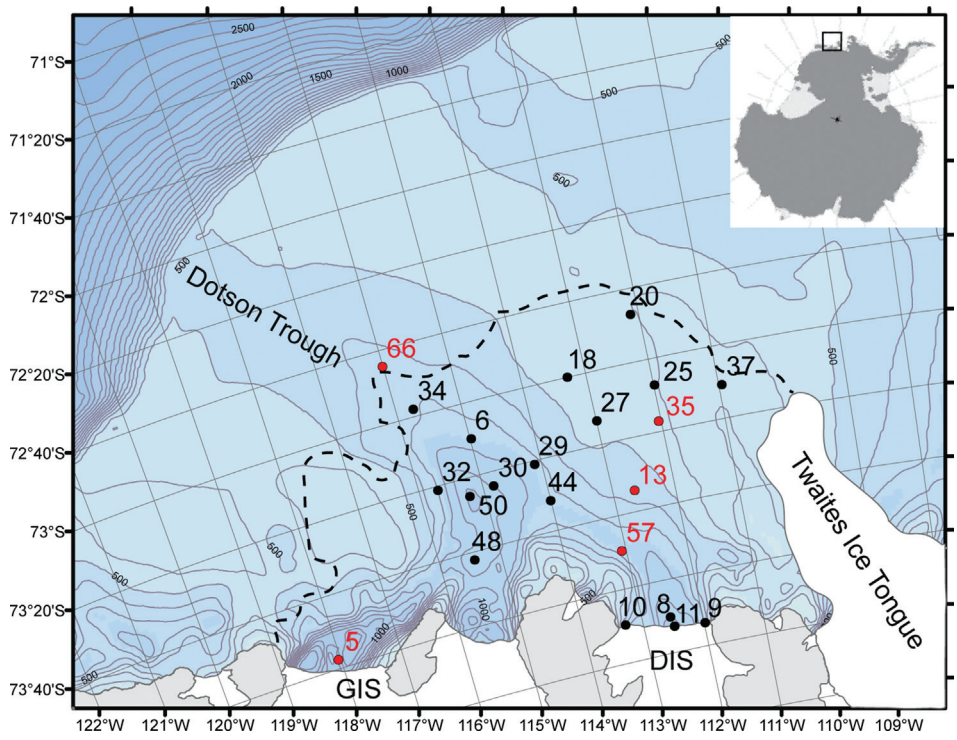

Figure 1

ASPIRE stations in the Amundsen Sea Polynya.

Hydrographic stations sampled during the ASPIRE cruise are projected on the Amundsen Sea Polynya (ASP) bathymetry. Fe addition bioassay experiments were performed at red stations; the water column was sampled at all stations. The dashed line shows the sea ice edge on 1 January 2011; the Getz Ice Shelf (GIS), Dotson Ice Shelf (DIS), and Twaites Ice Tongue are shown in white. Inset shows the location of the ASP in Antarctica.

doi: 10.12952/journal.elementa.000043.f001

Phytoplankton photoacclimate to low light by increasing their cellular pigment concentration to maximize the capture of photons (Falkowski and LaRoche, 1991; MacIntyre et al., 2002). However, Fe availability affects photoacclimation because biosynthesis of pigments requires Fe and the photosynthetic apparatus has a high Fe content (Raven, 1990; Greene et al., 1992). Thus, phytoplankton in low Fe regions may be impaired in their ability to photoacclimate (Greene et al., 1992; Vassiliev et al., 1995) or may have adapted mechanisms to increase the capture of photons without increasing Fe requirements (Strzepek and Harrison, 2004; Strzepek et al., 2012).

In this study, we investigated the effects of Fe additions on phytoplankton growth and photosynthesis rates during the build-up phase of a phytoplankton bloom in the ASP and assessed how Fe availability affected phytoplankton photoacclimation. We measured phytoplankton biomass, photosynthetic parameters, and productivity rates in surface waters of the ASP (Figure 1) and performed Fe addition bioassay experiments throughout the ASP to test effects of Fe additions on these parameters. In addition, effects of Fe addition on bacterial productivity were evaluated in the experiments. Moreover, interactions between Fe and light availability were tested in the experiments by including incubations at different light levels. Experimental results were then used to draw conclusions about Fe limitation of phytoplankton photosynthesis and productivity in the ASP.

Methods

Sampling

Seawater samples were collected during the NBP 10-05 cruise on the RVIB *Nathaniel B. Palmer* in the ASP during the austral spring and summer, 13 December 2010 to 12 January 2011. Water for analysis of parameters listed in the section on *Analytical methods* was sampled from discrete depths in the upper 300 m of the water column at 22 stations (Figure 1) during the middle of the day within three hours of solar noon. Water was sampled with trace metal clean (TMC) techniques using externally-closing 12 L Niskin bottles (Model 110BES, Ocean Test Equipment, Ft. Lauderdale, FL, USA) mounted on a GEOTRACES-style non-contaminating CTD-Rosette deployed on a coated aramid cable (see Sherrell et al., 2015, for details). Continuous vertical profiles of temperature, salinity, irradiance, fluorescence, and suspended particle abundance were obtained from the water column using a SeaBird 911+ CTD, a Chelsea fluorometer, photosynthetically active radiation (PAR) sensor (Biospherical), and a 25-cm WETLabs transmissometer, respectively, mounted on a TMC rosette.

Fe addition bioassay experiments

At five stations (Figure 1), large volumes of seawater (~ 100 L) were collected at select depths (see below) within the upper 50 m of the water column for bioassay experiments to study the effects of Fe addition under different light conditions, using TMC techniques throughout the experiments. Acid-washed polycarbonate bottles (2 L) were rinsed three times with MilliQ water and once with seawater from the same station before being filled to the brim with unfiltered seawater. Triplicate bottles for each treatment were incubated at in-situ water temperature in transparent deck incubators under incident irradiance shaded with different levels of neutral transmission screening. $FeCl_3$ was added to the Fe treatments from a 1000x stock in weakly acidified, 0.2 µm filtered seawater, in a final concentration of 4 nmol L^{-1} (Mills et al. 2012). Nothing was added to the control treatments. Bottles were capped and caps were wrapped with parafilm to prevent contamination by water from the incubator. All treatments were sampled within three hours of solar noon at the beginning of the experiment (T = 0 days), at 4 days, and at 7 or 8 days for all parameters listed in the section on *Analytical methods*. At three of the five stations (Stations 5, 13, and 35), parallel experiments were conducted with water from two different depths, the surface (S: 8–12 m) and subsurface (deep, D: 35–50 m). Water from each depth was incubated at 10% of incident irradiance. At the two remaining stations (Stations 57 and 66), only surface water was incubated in three parallel experiments under different light conditions: high (50%), medium (10%), and low (1%) incident irradiance.

Analytical methods

Nutrients and iron concentrations

Concentrations of nitrate (NO_3), ammonium (NH_4), phosphate (PO_4) and silicate ($Si(OH)_4$) from seawater samples at 22 stations and bioassay experiments were determined by flow injection analysis using a Lachat Instruments Quickchem 8000 Autoanalyzer according to standard protocols (see Vernet et al., 2011). Samples were collected directly from the experimental bottles, filtered through 0.2 µm Acrodisc® filters and stored at 4°C until analysis on the same day.

Concentrations of DFe from seawater samples at 16 stations and T = 0 samples of the bioassay experiments were determined by preconcentration and isotope dilution ICP-MS and are described in full in Sherrell et al. (2015). Concentrations of particulate Fe (PFe) from seawater samples at 11 stations and T = 0 samples of the bioassay experiments were determined by ICP-MS by methods following Planquette and Sherrell (2012) and have been reported elsewhere (Harazin et al., 2014).

Particulate organic carbon (POC) and particulate organic nitrogen (PON)

Duplicate samples from the bioassay experiments (100–1000 ml) were filtered onto precombusted (450°C for 4 h) 25 mm Whatman GF/F filters and dried at 60°C for analysis of POC and PON on a Carlo-Erba NA-1500 elemental analyzer using acetanilide as a calibration standard.

The POC concentrations at T = 0 and at 4 days were used to calculate phytoplankton growth rates (µ: d^{-1}) in the bioassay experiments using the equation:

$$POC_{T4} = POC_{T0}e^{\mu T}. \quad (1)$$

Pigment analysis

Seawater samples at 19 stations and bioassay experiment samples (50–500 mL) for chlorophyll *a* (Chl *a*) were filtered onto 25 mm Whatman GF/F filters, extracted overnight at 4°C in 5 mL of 90% acetone, and analyzed on a Turner Model 10AU fluorometer before and after acidification (Holm-Hansen et al., 1965).

The full pigment composition was analyzed for seawater samples at 12 stations and T = 0 samples of the bioassay experiments by High Performance Liquid Chromatography (HPLC). Samples (100–2000 mL) were filtered onto 25 mm Whatman GF/F filters, flash-frozen in liquid N_2, and stored at –80°C until analysis. Filters were extracted for two hours in 98% methanol: 2% ammonium acetate [vol:vol] in the dark at –20°C after disruption by sonication. Pigments were separated on a SPD-M10AVP HPLC system (Shimadzu, Inc.) using a Agilent 4.6 x 250 mm C18 column kept at 30°C according to Wright et al. (1991), using standards for Chl *a*, chlorophyll *b* (Chl *b*), chlorophyll c_3 (Chl c_3), peridinin (Per), 19′-butanoyloxylfucoxanthin (19′-But), fucoxanthin (Fuc), 19′-hexanoyloxyfucoxanthin (19′-Hex), neoxanthin (Neo), prasinoxanthin (Pras), violaxanthin (Viol), alloxanthin (Allo), lutein (Lut), antheraxanthin (Anth), diadinoxanthin (Diad), diatoxanthin (Diat), and β-carotene (β-Car). The Chl *a* breakdown product chlorophillide *a* was detected in few samples at < 2% of Chl *a* concentrations.

The ratios of the first 12 of these pigments were used to determine the phytoplankton class abundance using the CHEMTAX analysis package, version 1.95 (Mackey et al., 1996; Wright et al., 1996). The initial input ratios (Table 1A) consisted of specific pigment ratios for eight phytoplankton classes that generally dominate Antarctic waters (Wright et al., 2010), including prasinophytes, chlorophytes, cryptophytes, diatoms (with a separate class for Chl c_3 containing diatoms such as *Pseudonitzschia*), dinoflagellates, and two classes of

Table 1A. Initial pigment: Chlorophyll *a* (Chl *a*) ratios used in the CHEMTAX analysis of pigment data[a]

Phytoplankton class	Pigment used in ratio with Chl *a*										
	Chl c_3	Lut	Per	19′-But	Fuc	19′-Hex	Neo	Pras	Allo	Viol	Chl *b*
Prasinophytes	0	0.006	0	0	0	0	0.030	0.315	0	0.056	0.620
Chlorophytes	0	0.220	0	0	0	0	0.062	0	0	0.031	0.180
Cryptophytes	0	0	0	0	0	0	0	0	0.220	0	0
Diatoms	0	0	0	0	0.520	0	0	0	0	0	0
Pseudonitzschia	0.033	0	0	0	0.610	0	0	0	0	0	0
P. antarctica H	0.130	0	0	0.010	0.080	0.400	0	0	0	0	0
P. antarctica L	0.270	0	0	0.001	0.010	1.100	0	0	0	0	0
Dinoflagellates	0	0	1.060	0	0	0	0	0	0	0	0

doi:10.12952/journal.elementa.000043.t001a

Table 1B. Optimized pigment: Chl *a* ratios after CHEMTAX analysis[a]

Phytoplankton class	Pigment used in ratio with Chl *a*										
	Chl c_3	Lut	Per	19′-But	Fuc	19′-Hex	Neo	Pras	Allo	Viol	Chl *b*
Prasinophytes	0	0.006	0	0	0	0	0.030	0.094	0	0.056	0.620
Chlorophytes	0	0.220	0	0	0	0	0.062	0	0	0.031	0.180
Cryptophytes	0	0	0	0	0	0	0	0	0.220	0	0
Diatoms	0	0	0	0	0.520	0	0	0	0	0	0
Pseudonitzschia	0.033	0	0	0	0.624	0	0	0	0	0	0
P. antarctica H	0.201	0	0	0.010	0.080	0.284	0	0	0	0	0
P. antarctica L	0.098	0	0	0.001	0.010	1.493	0	0	0	0	0
Dinoflagellates	0	0	1.060	0	0	0	0	0	0	0	0

[a]Abbreviations: Chl c_3 = chlorophyll c_3, Lut = lutein, Per = peridinin, 19′-But = 19′-butanoyloxyfucoxanthin, Fuc = fucoxanthin, 19′-Hex = 19′-hexanoyloxyfucoxanthin, Neo = neoxanthin, Pras = prasinoxanthin, Allo = alloxanthin, Viol = violaxanthin, Chl *b* = chlorophyll *b*.
doi: 10.12952/journal.elementa.000043.t001b

P. antarctica. The two classes of *P. antarctica* account for variations in pigment ratios between strains (Zapata et al., 2004) and changes in response to Fe limitation (Van Leeuwe and Stefels, 2007, DiTullio et al., 2007, Alderkamp et al., 2012b). The pigment ratios in the output matrix (Table 1B) were within those reported in the literature (Zapata et al., 2004, Van Leeuwe and Stefels, 2007, DiTullio et al., 2007, Wright et al., 2010, Alderkamp et al., 2012b). Diatoms and *Pseudonitzschia* are presented together as diatoms and the two *P. antarctica* classes are presented together as *P. antarctica.*

Phytoplankton photosynthesis rates

Photosynthesis vs irradiance (*P-E*) relationships were determined in surface water samples (2–10 m depth) at 12 stations and in one sample from pooled replicates for each incubation treatment. *P-E* relationships were determined using the ^{14}C-bicarbonate incorporation technique by incubating 2 mL aliquots of seawater in a photosynthetron for two hours over a range of 20 different light intensities ranging from 3 to 542 µmol photons m^{-2} s^{-1} at 0°C (Lewis and Smith, 1983; the full method is outlined in Arrigo et al., 2010). CO_2 incorporation normalized by Chl *a* concentration was calculated from radioisotope incorporation and the data were fit by least squares nonlinear regression to the equation of Webb et al. (1974):

$$P^* = P^*_{\max}\left(1-exp\left(-\alpha^*\frac{E}{P^*_{\max}}\right)\right) \quad (2)$$

where P^*_{max} is the maximum rate of photosynthesis (CO_2 incorporation in g C g^{-1} Chl *a* hr^{-1}) and α^* is the initial slope of the *P-E* curve (g C g^{-1} Chl *a* hr^{-1} [µmol photons m^{-2} s^{-1}]$^{-1}$) where photosynthesis rates are light-limited. The photoacclimation parameter, E_k, was calculated as P^*_{max}/α^*. *P-E* data were also fitted to the model of Platt et al. (1980), which contains the photoinhibition parameter ß* (g C g^{-1} Chl *a* hr^{-1} [µmol photons m^{-2} s^{-1}]$^{-1}$). However, ß* was not significantly different from zero in any of the *P-E* curves and, therefore, this model was disregarded.

Phytoplankton optical absorption (ā*)
The spectrally averaged optical absorption cross section ($\overline{a}^*$, m^2 mg^{-1} Chl *a*) was determined in surface water samples (2–10 m depth) at 12 stations and in one sample from pooled replicates for each bioassay incubation treatment. Aliquots of the seawater sample (100–1000 mL) were filtered onto 25 mm Whatman GF/F filters for measurement of particulate absorption spectra (a_p, 300–800 nm) and detrital absorption (a_{det}, 300–800 nm) on a Perkin-Elmer Lambda 35 spectrophotometer equipped with an integrating sphere (Labsphere) using the filter pad method and optical corrections in Mitchell and Kiefer (1988) and the coefficients of Bricaud and Stramski (1990). Detrital absorption (a_{det}, 300–800 nm) was assayed after methanol extraction according to the method of Kishino et al. (1985). Chl *a*-specific optical absorption cross sections (a^*_{ph}) at each wavelength (λ) were calculated as:

$$a^*_{\mathrm{ph}}(\lambda) = \frac{a_{\mathrm{p}}(\lambda) - a_{\mathrm{det}}(\lambda)}{[Chla]} \tag{3}$$

where [*Chla*] is the Chl *a* concentration of the sample.

Spectrally averaged Chl *a*-specific optical absorption cross sections ($\overline{a}^*$, m^2 mg^{-1} Chl *a*) were calculated using the equation:

$$\overline{a}^* = \frac{\sum_{\lambda=400}^{\lambda=700} a^*_{ph} E(\lambda)}{\sum_{\lambda=400}^{\lambda=700} E(\lambda)} \tag{4}$$

where $E(\lambda)$ (μmol photons m^{-2} s^{-1}) is the spectral irradiance of the photosynthetron light source.

Quantum yield of photosynthesis
The quantum yield of photosynthesis (Φ_m in C mol^{-1} photons) was calculated as:

$$\Phi_m = \frac{\alpha^*}{43.2\overline{a}^*} \tag{5}$$

after first confirming that Φ_m was maximal at the lowest light level used in each of the assays (Johnson and Barber, 2003).

Variable fluorescence
A Satlantic Fluorescence Induction and Relaxation (FIRe) system was used to determine the maximum photochemical efficiency (F_v/F_m) and the functional absorption cross section (σ_{PSII}) ($Å^2$ $photon^{-1}$) of photosystem II (Gorbunov et al., 1999) for water samples at 11 stations and bioassay experiment samples. Prior to analysis, the FIRe was blanked with GF/F-filtered seawater from the same station. After sampling from the sample bottles, samples were acclimated in the dark at 2°C for 30 min to fully oxidize the photosynthetic reaction centers.

Bacterial productivity
Bacterial productivity was estimated in the bioassay experiments from incorporation of ^{3}H-leucine into protein (Williams et al., 2015). Each of the incubation bottles served as a replicate in the measurements.

Water column analysis

Diffuse attenuation coefficient
The diffuse attenuation coefficient of downwelling PAR (K_d) in the water column was determined by fitting the equation:

$$E_z = E_0\, e^{-Kd^*z} \tag{6}$$

to each PAR profile, where E_z is the irradiance at depth z and E_0 is the irradiance just below the sea surface.

Mixed layer depth (MLD)
The MLD was determined from each CTD profile as the shallowest depth at which the density (σ_T) was 0.02 kg m^{-3} greater than at the surface (Cisewski et al., 2008; Alderkamp et al., 2012a).

Mean light level in the mixed layer (E_{UML})
To calculate the mean daily PAR in the upper mixed layer (E_{UML}, mol photons m^{-2} day^{-1}), we used the equation of Riley (1957):

$$E_{UML} = \frac{\overline{E}_{surf}\, T\left(1-e^{-K_d z_{UML}}\right)}{K_d z_{UML}} \quad (7)$$

where $\overline{E}_{surf}$ is the total daily surface PAR averaged over five days and T is the mean transmittance through the sea surface (0.85 for open water, 0.20 for grey ice and nilas, and 0.05 for snow covered and multiyear ice).

Water column productivity
Phytoplankton productivity throughout the water column was estimated at each station from the Chl *a* concentrations, light availability in the water column, and *P-E* parameters, as described in Alderkamp et al. (2012a). Briefly, at depth intervals of 1 m, Chl *a* concentrations were estimated from continuous vertical fluorescence profiles that were calibrated to the measured Chl *a* concentrations at similar depths (Chl *a* = 0.71 fluorescence; R^2 = 0.69). The daily light cycle was binned in 10-min intervals and the mean over the previous five days was used to estimate the sinusoidal light cycle at 1-m depth intervals at each station based on the measured K_d of that station. These light levels were then used to calculate the phytoplankton productivity at each depth using *P-E* parameters of the phytoplankton collected at 10 m depth. These *P-E* parameters were assumed to be representative of phytoplankton in the upper mixed layer (UML) where > 99% of the phytoplankton productivity occurred (virtually no light penetrated below the MLD because the high phytoplankton biomass levels resulted in high K_d in all stations).

Statistical analysis

Effects of Fe addition were tested by comparing Fe addition treatments to unamended controls in each bioassay experiment using one-way ANOVA analysis. All parameters for phytoplankton photosynthesis and cellular composition, as well as bacterial productivity, were tested at day four to eliminate potential effects of NO_3 limitation (see *Phytoplankton biomass response to Fe addition*). Interactions between Fe addition and original sample depth, as well as interactions between Fe addition and light availability, were tested using two-way ANOVA analysis. Differences were considered significant at $p < 0.05$. Simple linear regression was used to test relationships between phytoplankton parameters in seawater samples.

Results

Phytoplankton bloom characteristics

The physical properties of the upper water column, which affected the Fe and light availability to the phytoplankton, varied markedly within the ASP (Randall-Goodwin et al., 2015). In the southern ASP, near the ice sheets, AASW was relatively salty, due to little overall sea ice or near surface glacial melt, and/or enhanced mixing with WW, as observed in the southwest ASP close to the Getz Ice Shelf (GIS) (e.g., Station 5, Figure 2), or due to enhanced mixing with meltwater-laden mCDW waters as observed in front of the Dotson Ice Shelf (DIS) and at Station 57 (Figure 2). In the central ASP, AASW was moderately fresh, due to less recent sea ice melt and/or wind mixing (e.g., Stations 13 and 35, Figure 2). In the northern ASP, AASW was very fresh due to recent sea ice melt, as observed along the sea ice edge and in the MIZ (e.g., Station 66, Figure 2). These surface water characteristics affected the phytoplankton throughout our sampling during the buildup of a dense spring-summer phytoplankton bloom that typically peaks in mid-January (Arrigo et al., 2012). The phytoplankton biomass increased over the course of the cruise (Yager et al., 2012), conforming to this typical bloom development.

Near the Getz Ice Shelf
The salty AASW with the largest contribution of WW was observed in the southwest ASP close to the GIS (Station 5; Table 2A) and had a MLD of ~ 35 m (Figure 3C), resulting in moderate light levels in the UML (E_{UML} 158 µmol photons m^{-2} s^{-2}). DFe in these surface waters were > 0.18 nmol L^{-1} (Figure 3E), whereas PFe was two orders of magnitude higher than DFe at > 18 nmol L^{-1} (Figure 3F). Phytoplankton biomass was 2.3 mg Chl *a* m^{-3} in surface waters (Figure 3G) and 177 mg m^{-2} integrated over depth (Figure 3H). The phytoplankton community was dominated by *Phaeocystis antarctica*, but diatoms and prasinophytes were also present and constituted up to 12% of the phytoplankton community at different depths (Table 2B, Figures 3I, 3J). Of the five stations sampled for the Fe addition bioassay experiments (see *Phytoplankton biomass response to Fe addition*), Station 5 is the most representative of salty AASW with WW influence (Figure 2).

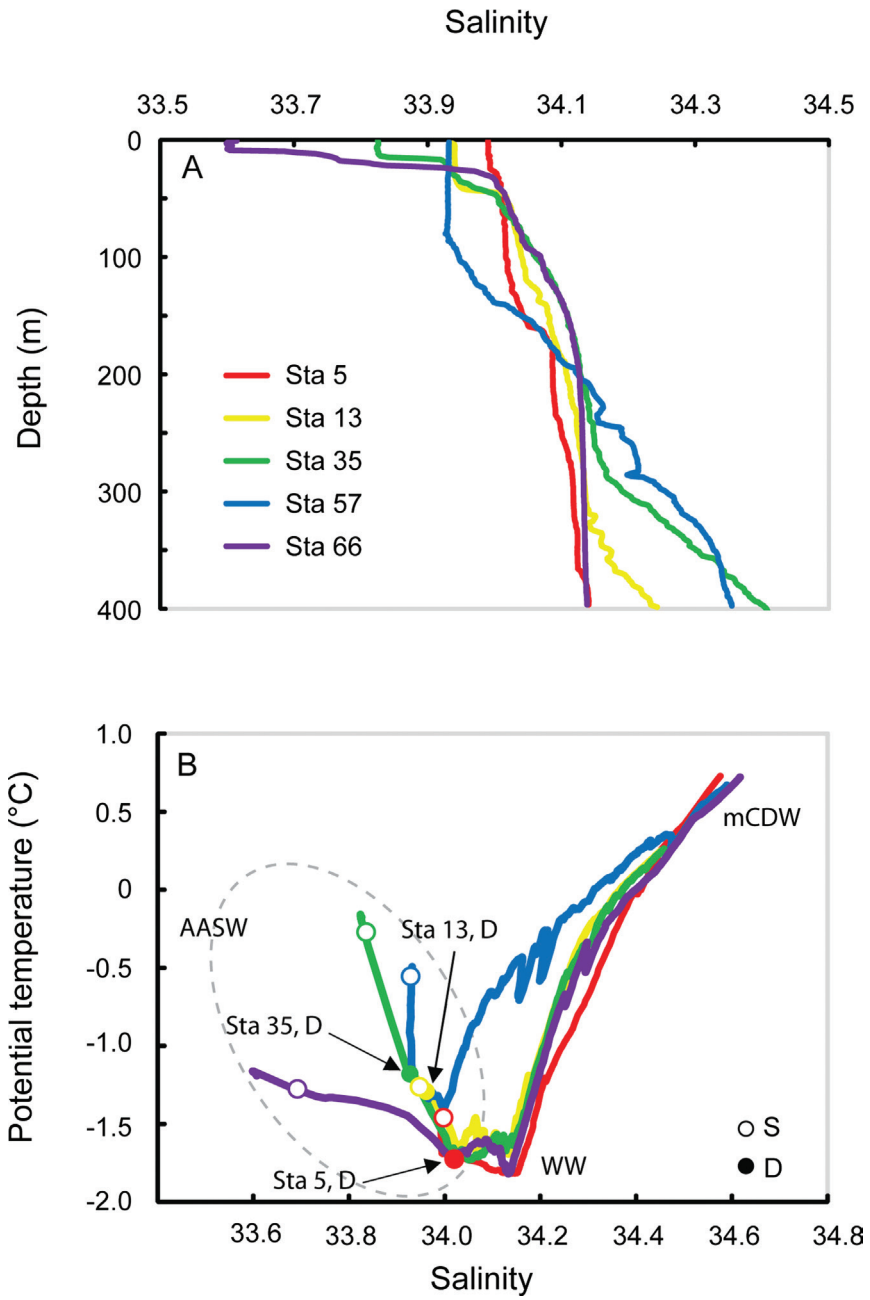

Figure 2

Water properties of Fe addition bioassay experiment stations.

Depth profiles of salinity are shown in (A), and temperature and salinity properties in (B), where AASW is Antarctic Surface Water, WW is Winter Water, and mCDW is modified Circumpolar Deep Water. Open symbols indicate surface waters (10 m depth); solid symbols indicate deeper subsurface waters (D, 35–50 m depth).

doi: 10.12952/journal.elementa.000043.f002

Near the Dotson Ice Shelf

Salty AASW with the largest contribution of mCDW was observed in the southern ASP close to the DIS (Stations 8, 9, 10, 11, and 57). The buoyancy-driven upwelling of mCDW destabilized the upper water column resulting in deep MLDs (40 to 70 m, Figure 3C). The deep MLD, in combination with variable light attenuation due to variable phytoplankton biomass, resulted in variable E_{UML} (50 to 220 µmol photons m^{-2} s^{-2}, Figure 3D). The meltwater-laden mCDW flowing from under the DIS appears to be the main source of DFe and PFe to the ASP (Sherrell et al., 2015) and the salty AASW contained 0.11–1.31 nmol L^{-1} DFe (Figure 3E) and 15–50 nmol L^{-1} PFe (Figure 3F). Phytoplankton biomass was <2.0 mg Chl *a* m^{-3} in surface waters (Figure 3G) and < 200 mg Chl *a* m^{-2} integrated over depth near the face of the DIS where the mCDW signature was strongest. At Station 57, approximately 50 km away from the DIS, surface Chl *a* increased to 8.6 mg m^{-3} (Figure 3G) and depth-integrated Chl *a* to 618 mg m^{-2} (Figure 3H).

Table 2A. Oceanographic data on water samples used to initiate bioassay experiments

Type of data	Station-specific data							
Station	**5**		**13**		**35**		**57**	**66**
Latitude (°S)	73°57.72		73°34.22		73°16.78		73°43.69	72°44.45
Longitude (°W)	118°01.18		112°40.03		112°06.28		113°15.20	116°01.21
Date	14 Dec 2010		19 Dec 2010		26 Dec 2010		1 Jan 2011	5 Jan 2011
Mixed layer depth (m)	28		42		22		80	25
Mean irradiance during experiment (μmol photons m^{-2} s^{-1})	1243		932		1098		1082	776
Sample type (surface, S; deeper subsurface, D)	**S**	**D**	**S**	**D**	**S**	**D**	**S**	**S**
Sample depth (m)	8.8	50.3	9.9	40.0	12.0	35.0	9.9	10.2
Salinity	34.01	34.05	33.94	33.94	33.83	33.93	33.93	33.69
Temperature (°C)	−1.46	−1.71	−1.25	−1.25	−0.26	−1.23	−0.55	−1.33
NO_3 (μmol L^{-1})	26.3	26.7	21.1	24.8	12.5	22.0	24.9	15.8
PO_4 (μmol L^{-1})	1.76	1.78	1.33	1.61	0.88	1.49	1.67	1.18
$Si(OH)_4$ (μmol L^{-1})	88.0	93.0	77.9	83.8	70.8	72.5	96.5	74.1
DFe (nmol L^{-1})	0.18	0.30	0.09	0.22	0.32	0.20	0.10	0.116
PFe (nmol L^{-1})	18.88	12.54	ND	ND	7.28	6.78	21.07	15.43

doi: 10.12952/journal.elementa.000043.t002a

Table 2B. Biological data on water samples used to initiate bioassay experiments[a]

Type of data	Station 5		Station 13		Station 35		Station 57	Station 66
	S	D	S	D	S	D	S	S
Chl *a*	3.8	3.7	8.4	6.5	14.0	7.4	5.6	10.8
POC	244	179	386	287	903	471	237	544
POC/Chl *a*	65.4	48.5	46.4	44.4	66.8	63.7	42.7	51.1
POC/PON	7.05	4.50	5.66	6.20	7.79	6.02	5.32	5.66
F_v/F_m	0.49	0.46	0.35	0.39	0.27	0.39	0.40	0.36
σ_{PSII}	525	561	737	677	608	648	544	638
P^*_{max}	3.52	3.00	2.97	2.61	2.27	2.92	3.18	2.48
α^*	0.080	0.065	0.051	0.058	0.034	0.075	0.032	0.067
E_k	44	46	58	45	67	39	99	37
$\bar{a}^*$	0.015	0.008	0.013	0.011	0.014	0.014	0.013	0.010
Φ_m	0.127	0.191	0.091	0.123	0.057	0.128	0.060	0.119
Dominant phytoplankton (fraction of total)	*Phaeocystis antarctica* (0.80)	*P. antarctica* (0.85)	*P. antarctica* (0.87)	*P. antarctica* (0.88)	*P. antarctica* (0.84)	*P. antarctica* (0.84)	*P. antarctica* (0.87)	*P. antarctica* (0.84)
2nd most abundant phyto-plankton	Prasinophytes (0.11)	Diatoms (0.11)	Prasinophytes (0.09)	Prasinophytes (0.08)	Prasinophytes (0.14)	Prasinophytes (0.15)	Diatoms (0.05)	Diatoms (0.11)
BP	6.4	5.6	63.6	55.6	74.1	61.7	49.5	89.6

[a] Abbreviations (and units): S = surface water sample, D = deeper subsurface sample, Chl *a* = Chlorophyll *a* (μg L^{-1}), POC = particulate organic carbon (μg L^{-1}), POC/Chl *a* (wt/wt), PON = particulate organic nitrogen, POC/PON (mol/mol), F_v/F_m = maximum photochemical efficiency of photosystem II (no units), σ_{PSII} = functional absorption cross section (Å $photon^{-1}$), P^*_{max} = maximum rate of photosynthesis (g C g^{-1} Chl *a* h^{-1}), α^* the initial slope of the photosynthesis versus irradiance curve (g C g^{-1} Chl *a* h^{-1} [μmol photons m^{-2} s^{-1}]$^{-1}$), E_k = photoacclimation parameter (μmol photons m^{-2} s^{-1}), $\bar{a}^*$ = spectrally averaged Chl *a*-specific optical absorption cross section (photons m^{-2}), Φ_m = quantum yield of photosynthesis (mol C mol^{-1} photons), BP = bacterial productivity (pmol Leu uptake L^{-1} h^{-1}).

doi: 10.12952/journal.elementa.000043.t002b

Central Amundsen Sea Polynya

In the center of the polynya, at increasing distance from the Dotson and Getz Ice Shelves (Stations 6, 18–32, 35–50), solar warming increased the temperature of AASW (–0.7 °C, Figure 3B) and recent sea ice melt lowered the salinity (< 33.9, Figure 3A). Both processes increase water column stratification, which decreased the MLD to 10–30 m (Figure 3C). The highest phytoplankton biomass was observed in the central ASP with

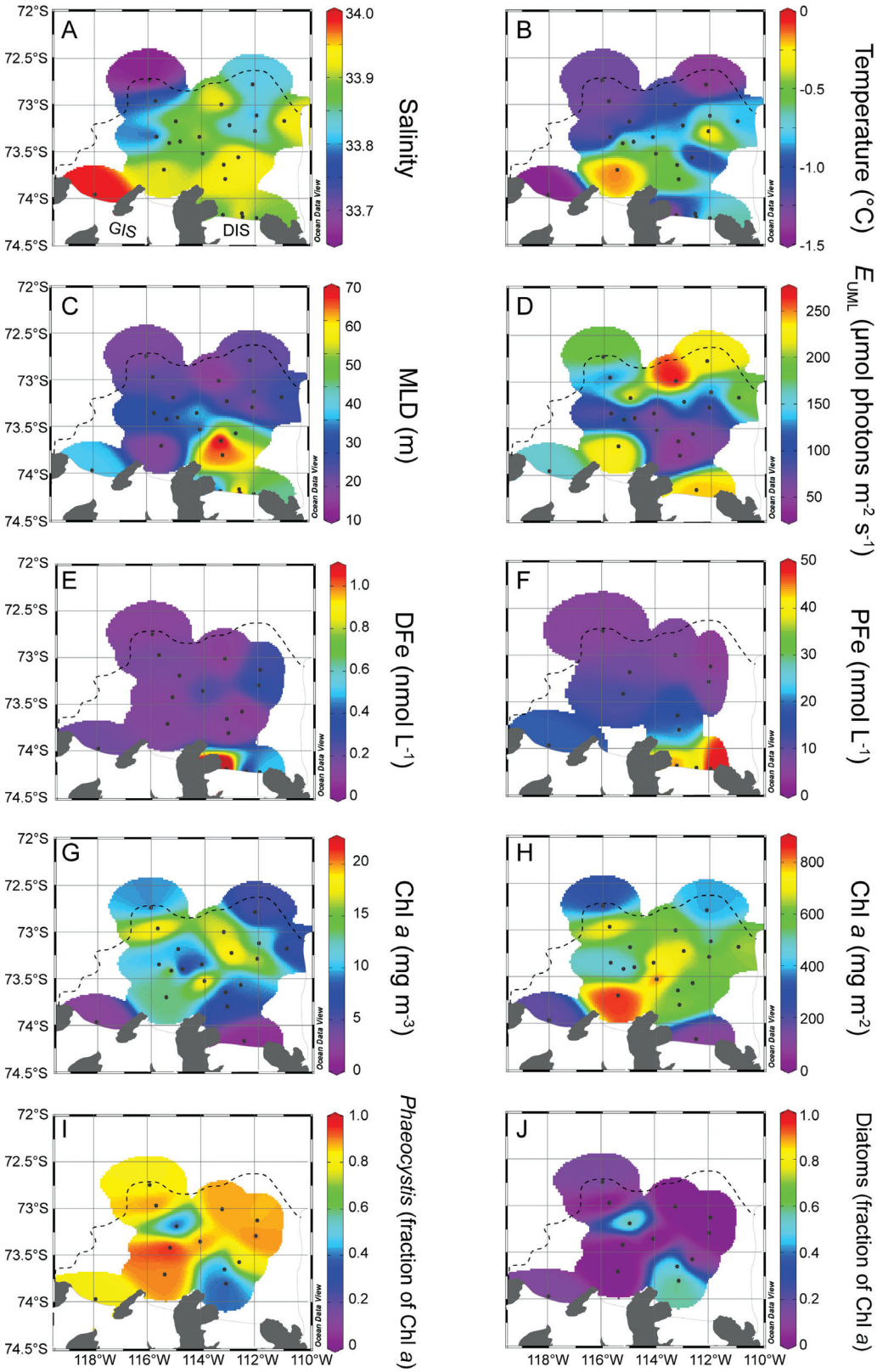

Figure 3

Surface water properties in the Amundsen Sea Polynya.

Properties shown for surface waters (2–10 m depth) are: salinity (A); temperature (B); mixed layer depth (MLD), the depth where density σ_t increased 0.02 from surface waters (C); E_{UML}, mean light in the upper mixed layer (D); dissolved Fe (DFe) concentrations in surface water (data from Sherrell et al., 2015) (E); particulate Fe (PFe) concentrations in surface waters (data from Harazin et al., 2014) (F); chlorophyll (Chl) *a* concentrations (G); depth-integrated Chl *a* (H); fraction of phytoplankton community as *Phaeocystis antarctica* (I); and fraction of phytoplankton community as diatoms (J). In each panel, the dashed line shows the sea ice edge on 1 January 2011 and the Getz Ice Shelf (GIS) and Dotson Ice Shelf (DIS) are shown in white.

doi: 10.12952/journal.elementa.000043.f003

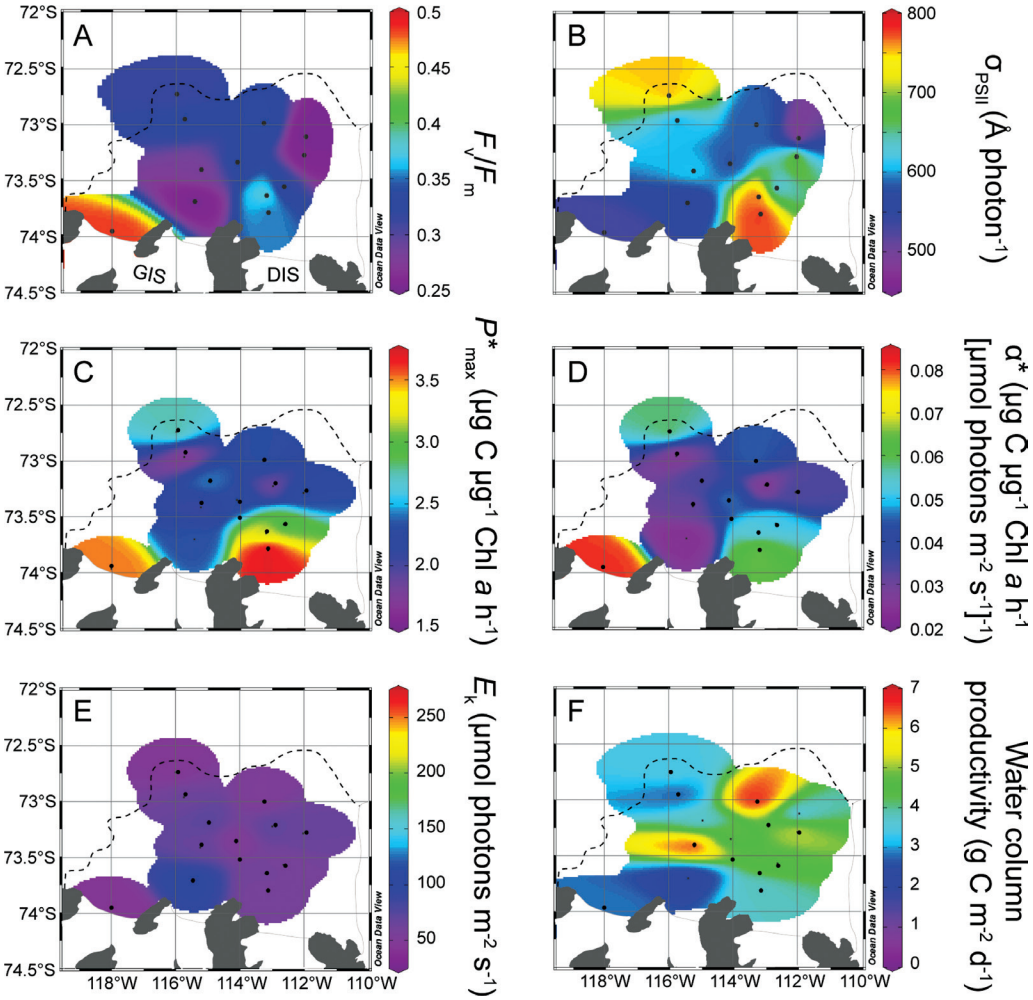

Figure 4

Photosynthetic parameters of surface phytoplankton.

Photosynthetic parameters shown for phytoplankton in surface waters (2–10 m depth) are: maximum photochemical efficiency of Photosystem (PS) II (F_v/F_m) (A), functional cross section of PS II (σ_{PSII}) (B), maximum photosynthesis rates normalized to chlorophyll *a* (Chl *a*) (P^*_{max}) (C), initial light-limited slope of the photosynthesis–irradiance normalized to Chl *a* (α*) (D), and photoacclimation parameter (E_k) (E). Water column productivity is shown in (F). In each panel, the sea ice edge on 1 January 2011, is shown by dashed line and the ice shelves are white: Getz Ice Shelf (GIS) and Dotson Ice Shelf (DIS).

doi: 10.12952/journal.elementa.000043.f004

mean surface Chl *a* of 12.6 ± 5.7 mg m^{-3} (Figure 3G) and mean depth-integrated Chl *a* of 604 ± 150 mg m^{-2} (Figure 3H). The highest Chl *a* concentrations were found in the upper 20 m of the water column, dropping to 5–10 mg m^{-3} at a depth of 20–50 m (Figure 5A). The shallow MLD, in combination with rapid light attenuation with depth due to the high phytoplankton biomass, resulted in a relatively low E_{UML} (< 50 µmol photons m^{-2} s^{-1}, Figure 3D). Moreover, the rapid light attenuation with depth resulted in a shallow euphotic zone with a 1% light depth shallower than the MLD. DFe and PFe in surface waters of the central polynya were on average 0.18 ± 0.07 nmol L^{-1} (Figure 3E) and 8.7 ± 3.6 nmol L^{-1} (Figure 3F), respectively. The phytoplankton community was dominated by *P. antarctica* at almost all stations throughout the central polynya. Diatoms contributed up to 60% to the phytoplankton biomass at two stations (Figures 3I, 3J), but contributed less or were almost absent at most stations. Prasinophytes were present in low numbers at most stations (< 10%) and contributed up to 14% to the phytoplankton community at some. The bioassay experiments at Stations 13 and 35 were conducted in the central ASP, where sea ice melt influence was stronger at Station 35 than at Station 13 (Figure 2).

Northern Amundsen Sea Polynya and Marginal Ice Zone (MIZ)

Very fresh AASW that was strongly affected by sea ice melt was found in the MIZ (Station 66) and in the northern waters of the ASP near the sea ice (Station 34). Sea ice melt waters were relatively fresh (< 33.85) and cold (< –1.5°C) (Figures 3A, 3B), but warmed over time. Freshening of surface waters by sea ice melt water increased stratification, which resulted in a shallow MLD (< 20 m, Figure 3C) and a relatively high E_{UML} > 150 µmol photons m^{-2} s^{-2} (Figure 3D). DFe in very fresh AASW was relatively low (0.11 ± 0.03 nmol L^{-1}; Figure 3E), as was PFe (6.9 ± 1.6 nmol L^{-1}; Figure 3F) when compared to other regions in the ASP. Phytoplankton biomass in very fresh AASW ranged from 6 to 10 mg Chl *a* m^{-3} (Figure 3G) and depth-integrated Chl *a* exceeded 400 mg m^{-2} (Figure 3H). All very fresh AASW stations were dominated by *P. antarctica*, although diatoms and prasinophytes were also present and constituted up to 4% and 13% of the phytoplankton assemblages, respectively. The bioassay experiment at Station 66 was situated in the MIZ where phytoplankton biomass was high, even though waters were still partially ice covered (Table 2B).

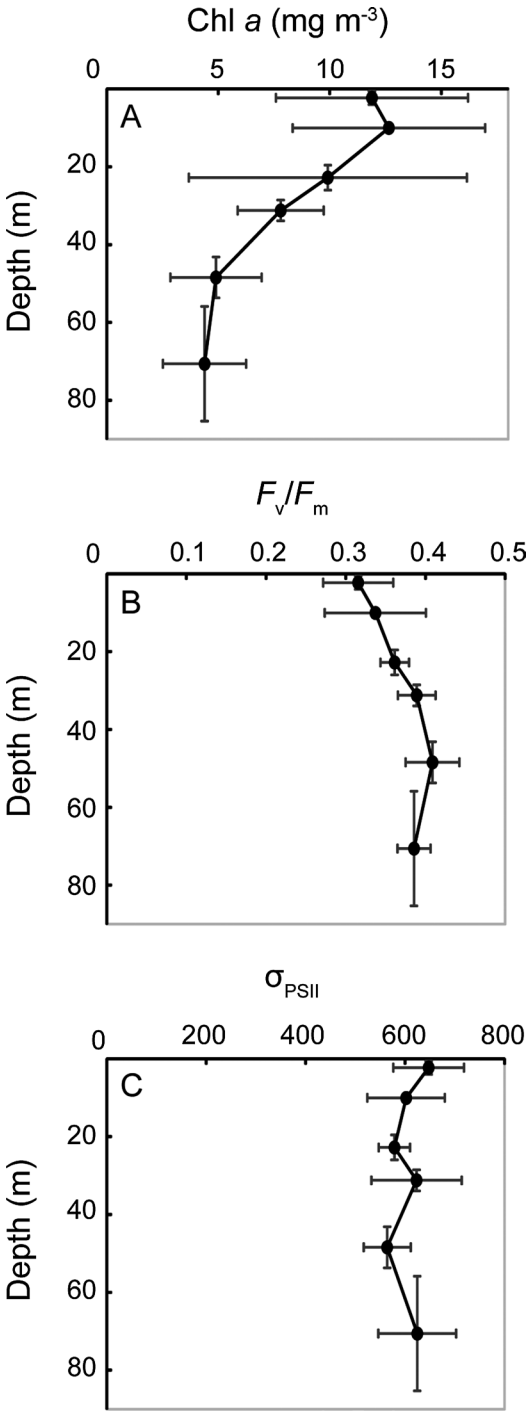

Figure 5

Depth profiles of phytoplankton variable fluorescence.

Mean and standard deviation of chlorophyll *a* (Chl *a*, n = 18) (A), maximum photochemical efficiency of Photosystem (PS) II (F_v/F_m, n = 14) (B), and functional cross section of PS II (σ_{PSII}, n = 14) (C) are shown with depth in the water column.

doi: 10.12952/journal.elementa.000043.f005

Phytoplankton photosynthesis in the ASP

Variable fluorescence parameters

In general, the F_v/F_m of phytoplankton was low in surface waters of the central ASP (< 0.35), and higher (> 0.4) in the salty AASW of the southern ASP near the DIS and GIS, at stations with a relatively strong WW and mCDW influence, respectively (Figure 4A). Phytoplankton in the very fresh AASW of the northern exhibited F_v/F_m values of 0.35. In general, F_v/F_m increased with depth in the upper 80 m of the water column (Figure 5B). The lowest F_v/F_m was observed in surface waters in the central ASP with the highest phytoplankton biomass. The relationship between F_v/F_m and Chl *a* in surface waters was negative (Table 3).

Table 3. Simple linear regressions for phytoplankton photosynthesis parameters in surface waters of the Amundsen Sea Polynya[a]

Variable 1	Variable 2	Equation	*n*	R^2	*p*
F_v/F_m	Chl *a*	F_v/F_m = –0.008 Chl *a* + 0.433	14	0.594	< 0.01
σ_{PSII}	Chl *a*		14	0.005	0.820
P^*_{max}	F_v/F_m	P^*_{max} = 8.84 F_v/F_m – 0.13	13	0.411	< 0.05
P^*_{max}	DFe		14	0.154	0.208
P^*_{max}	PFe	P^*_{max} = 0.09 PFe + 1.67	8	0.745	< 0.01
α^*	F_v/F_m	α^* = 0.26 F_v/F_m – 0.035	13	0.678	< 0.001
α^*	P^*_{max}	α^* = 0.02 P^*_{max} – 0.009	14	0.820	< 0.001
α^*	DFe		14	0.081	0.370
α^*	PFe	α^* = 0.002 PFe + 0.024	8	0.506	< 0.05
WCP	Chl *a*		11	0.001	0.928
WCP	Depth-integr Chl *a*		11	0.041	0.552
WCP	MLD		11	0.002	0.906
WCP	E_{UML}		11	0.059	0.473
WCP	P^*_{max}		11	0.043	0.538
WCP	α^*		11	0.037	0.571
WCP	DFe		11	0.005	0.829
WCP	PFe		8	0.063	0.548

[a] Abbreviations (and units): F_v/F_m = maximum photochemical efficiency of photosystem II (no units), Chl *a* = Chlorophyll *a* (μg L^{-1}), depth-integrated Chl *a* (mg m^{-2}), σ_{PSII} = functional absorption cross section (Å $photon^{-1}$), P^*_{max} = maximum rate of photosynthesis (g C g^{-1} Chl *a* h^{-1}), α^* = initial slope of photosynthesis versus irradiance curve (g C g^{-1} Chl *a* h^{-1} [μmol photons m^{-2} s^{-1}]$^{-1}$), DFe = dissolved iron (nmol L^{-1}), PFe = particulate iron (nmol L^{-1}), WCP = water column productivity (g C m^{-2} d^{-1}), MLD = mixed layer depth (m), E_{UML}= mean daily PAR in the upper mixed layer (mol photons m^{-2} day^{-1}).

doi: 10.12952/journal.elementa.000043.t003

The σ_{PSII} of phytoplankton was variable (500–900 Å $photon^{-1}$) throughout surface waters in the ASP (Figure 4B). The highest σ_{PSII} (800–900 Å $photon^{-1}$) was observed in salty AASW near the DIS, whereas the lowest (500 Å $photons^{-1}$) was observed close to the GIS (Figure 4B). The σ_{PSII} in the central polynya ranged from 473 to 938 Å $photon^{-1}$ and was similar to that in waters affected by sea ice melt. There was no trend in σ_{PSII} with depth (Figure 5C); moreover, there was no significant relationship between σ_{PSII} and Chl *a* (Table 3).

P-E parameters

The spatial distribution of P^*_{max} resembled that of F_v/F_m. P^*_{max} was highest in the salty AASW in the southern ASP near the DIS and GIS (Figure 4C), exceeding 3.0 μg C μg^{-1} Chl *a* h^{-1}. The P^*_{max} was lowest (< 2.0 μg C μg^{-1} Chl *a* h^{-1}) in the central ASP in the areas with the highest phytoplankton biomass. In fresh AASW waters affected by sea ice melt water, P^*_{max} was intermediate. There was no trend in P^*_{max} with depth (Table 1B). The relationship between P^*_{max} and F_v/F_m was positive (Table 3). There was no relationship between P^*_{max} and DFe, but a positive relationship between P^*_{max} and PFe was detected (Table 3).

The spatial distribution of α^* resembled that of P^*_{max}, with high α^* (> 0.06 μg C μg^{-1} Chl *a* h^{-1} [umol photons m^{-2} s^{-1}]) in the southern ASP near the DIS and GIS (Figure 4D) and low α^* (< 0.03 μg C μg^{-1} Chl *a* h^{-1} [umol photons m^{-2} s^{-1}]) in the central ASP. The parameter α^* was intermediate in fresh AASW affected by sea ice melt water in the northern ASP (Figure 4D). In general, α^* increased with depth (Table 2B). There were strong positive relationships between α^* and F_v/F_m, and between α^* and P^*_{max} (Table 3). There was no relationship between α^* and DFe, but the relationship between α^* and PFe was positive (Table 3).

The E_k ranged from 40 to 100 μmol photons m^{-2} s^{-1} (Figure 4E) and was generally lower than E_{UML} (Figure 4E). The strong positive relationship between P^*_{max} and α^* resulted in no spatial pattern in E_k, although E_k did decrease with depth (Table 2B).

Water column productivity in the ASP ranged from 2.0 to 6.5 g C m^{-2} d^{-1} (Figure 4F). In general, productivity was highest (> 5.0 g C m^{-2} d^{-1}) in the central polynya in waters with relatively shallow MLD (< 30 m) that resulted in high values for E_{UML} (> 130 μmol photons m^{-2} s^{-2}) and Chl *a* concentrations (> 7 mg m^{-3} and > 400 mg m^{-2}). Water column productivity depends on phytoplankton biomass, light availability, and *P-E* parameters of phytoplankton. However, productivity showed no relationship with any of these parameters, such as surface Chl *a,* depth-integrated Chl *a*, MLD, E_{UML}, P^*_{max}, or α^* (Table 3). Similarly, there was no relationship between productivity and DFe in surface waters or between productivity and PFe (Table 3).

Phytoplankton biomass response to Fe addition

In general, phytoplankton biomass increased significantly over the course of the incubation in all experiments at 10% and 50% irradiance (Figure 6, left panels). The increase in biomass was accompanied by a rapid drawdown of NO_3 (Figure 6, right panels), which was depleted by the end (7 or 8 days) in all incubations at 10% and 50% irradiance, both in the control and the Fe treatments (Figure 6, right panels). Moreover, all NO_3 was depleted by day 4 in both control and Fe treatments of surface water from Station 35, such that these incubations were likely NO_3-limited (Figure 6F).

Fe addition resulted in higher biomass compared to controls in four of the bioassay incubations in the ASP, whereas there was no significant effect of Fe in eight incubations (Figure 6). In the incubations of surface water from Station 5, in the salty AASW near the face of the GIS, Fe addition enhanced phytoplankton biomass 1.37-fold by day 4, which increased growth rate to 0.29 d^{-1} compared to 0.26 d^{-1} in the control (one-way ANOVA, $p < 0.05$, Table 4). By day 7, when NO_3 was depleted, biomass in the Fe treatment was still 1.27-fold higher than in the control treatment (one-way ANOVA, $p < 0.05$, Figure 6A). In the incubations of subsurface water from Station 35, in the moderately fresh AASW in the central ASP, Fe addition enhanced phytoplankton biomass 1.32-fold by day 4 (one-way ANOVA $p < 0.05$, Figure 6E), which increased the phytoplankton growth rates to 0.26 d^{-1} compared to 0.12 d^{-1} in the control (one-way ANOVA, $p < 0.05$, Table 4). By day 8, when NO_3 was depleted, biomass in the Fe treatment was still 1.13-fold higher than in the control treatment (one-way ANOVA, $p < 0.05$, Figure 6E). In the incubations of subsurface water from Station 57, in the salty AASW affected by mCDW, Fe addition enhanced biomass 1.14-fold in the 10% irradiance incubation by day 4 (one-way ANOVA, $p < 0.05$), which increased phytoplankton growth rates to 0.31 d^{-1} compared to 0.29 d^{-1} in the control (one-way ANOVA, $p < 0.05$, Table 4). By day 7, when NO_3 was depleted, Fe addition enhanced the biomass 1.42-fold in the 50% irradiance treatment (one-way ANOVA, $p < 0.05$, Figure 6G). Fe addition also enhanced NO_3 drawdown when compared to controls in two subsurface water incubations (Stations 13 and 35), whereas there was no significant Fe effect in the ten other incubations.

Interactions between effects of Fe and sample depth on phytoplankton growth rates and NO_3 drawdown were studied by analyzing data from day 4 of Stations 5, 13 and 35 bioassay experiments together (Table 5). Both growth rates and NO_3 drawdown were higher in the subsurface than surface water incubations over these three experiments (one-way ANOVA, $p < 0.05$). These results are likely due to NO_3-limitation in the incubations of surface water from Station 35, resulting in lower growth rates and NO_3 drawdown compared to subsurface water incubations that were not NO_3-depleted. There was no interaction between Fe and sample depth on phytoplankton growth rates, nor on NO_3 drawdown (Table 5).

Data from day 4 of the Stations 57 and Station 66 incubations were analyzed together to study interactions between Fe and light on phytoplankton growth rates and NO_3 drawdown (Table 5). Whereas both higher Fe and light availability individually increased the phytoplankton growth rates in the incubations (one-way ANOVA $p < 0.05$), there was no interaction between these factors. Similarly, there were no interactions between Fe and light effects on NO_3 drawdown (Table 5).

Phytoplankton photosynthesis response to Fe additions

Variable fluorescence responses

All photosynthesis responses to Fe additions were studied on day 4 of the incubations, when NO_3 was not depleted, except for the surface water incubation from Station 35. The F_v/F_m ranged from 0.25 to 0.48 (Figures 7A, 7B) and was in the same range as the initial F_v/F_m of surface phytoplankton (Figure 4A). Fe addition increased the F_v/F_m in almost all of the 10% and 50% irradiance incubations when compared to control treatments (one-way ANOVA, $p < 0.05$, Figures 7A, 7B) by an average of 1.17-fold, whereas there was no effect in the 1% irradiance incubations. Despite this trend, the interaction between Fe and light was not significant (Table 5) when experiments at Stations 57 and 66 were analyzed together, likely due to the small but significant decrease in F_v/F_m after Fe addition in the 10% irradiance incubation at Station 57 (Figure 7B). In addition, the original sampling depth did not affect the F_v/F_m in the incubations, nor was there an interaction between Fe and sample depth (Table 5).

The σ_{PSII} by day 4 of the incubations ranged from 442 to 765 Å $photon^{-1}$, which was within the range of the initial σ_{PSII} of the incubations (Table 2B) and that of surface phytoplankton in the ASP (Figure 4B). Fe effects on σ_{PSII} were inconsistent (Figures 7C, 7D), reducing σ_{PSII} in two incubations (Stations 5, S incubation; Station 57, 10% irradiance incubation), increasing σ_{PSII} in another incubation (Station 13, D incubation), and not affecting σ_{PSII} in the remaining incubations (Figures 7C, 7D). Analyzing all incubations together revealed no overall Fe effect on σ_{PSII} (Table 5). The σ_{PSII} of the surface water incubations was slightly higher than the subsurface water incubations, but this effect was not significant (Table 5). Moreover, there was no interaction between effects of Fe and sample depth (Table 5). Light did not affect σ_{PSII}, but there was a significant interaction between Fe and light (two-way ANOVA, $p < 0.05$), where Fe addition slightly decreased σ_{PSII} at low light, but did not affect σ_{PSII} at high light (Figure 7D).

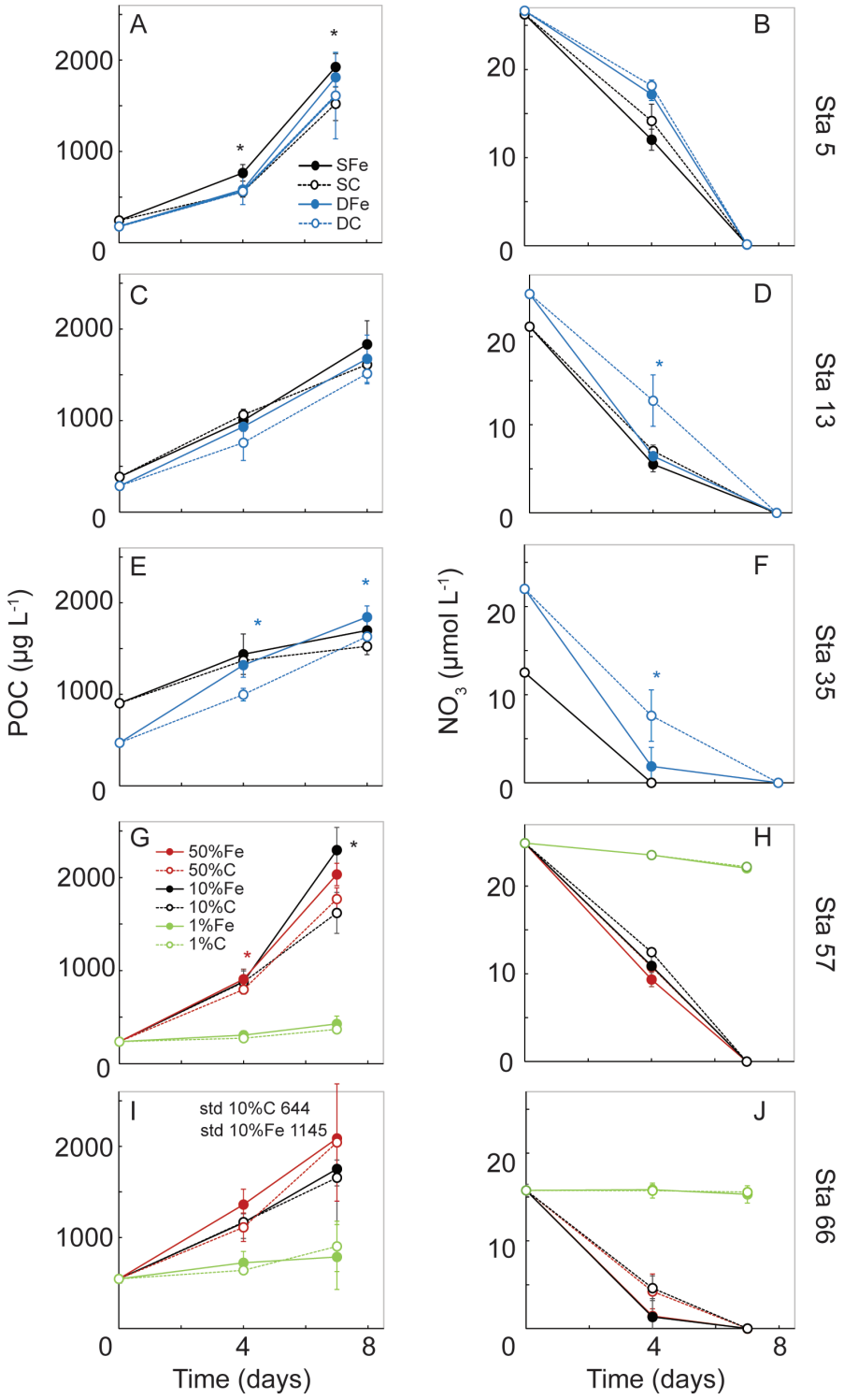

Figure 6

Phytoplankton responses to iron addition.

Mean and standard deviation of the measured parameters are shown for triplicate incubations of Fe additions (solid symbols) and unamended controls (open symbols). Left panels indicate change in biomass (particulate organic carbon: POC) over time of incubation; right panels indicate change in nitrate (NO_3). The upper three rows of panels show responses during incubation of surface (black) and deeper subsurface (blue) waters from Station 5 (A, B) near the Dotson glacier, Station 13 (C, D) in the central Amundsen Sea Polynya (ASP), and Station 35 (E, F) in the central ASP. The lower two rows of panels show responses at different levels of incident irradiance (1%, green; 10%, black; 50%, red) for surface waters from Station 57 (G, H) close to the Dotson Ice Shelf and Station 66 (I, J) in the marginal ice zone (MIZ). An asterisk indicates significant difference between Fe addition and control of the same color at the time of sampling (one-way ANOVA, $p < 0.05$). In (F), data for SC are identical to data for SFe.

doi: 10.12952/journal.elementa.000043.f006

Photosynthesis vs irradiance (P-E) parameters

High P^*_{max} exceeding 2.2 µg C µg^{-1} Chl *a* h^{-1} were observed in all incubations by day 4 (Figures 8A, 8B). Fe addition increased P^*_{max} compared to controls in almost all incubations, on average 1.31-fold. This increase was greatest in the experiments where Fe also affected phytoplankton growth (S for Station 5, D for Station 35), with P^*_{max} increasing 1.75-fold and 1.56-fold, respectively. P^*_{max} was lowest for surface water incubations from Station 35, where NO_3 was depleted by day 4. When experiments were analyzed together, the Fe effect on P^*_{max} was significant (Table 5, one-way ANOVA, $p < 0.05$). The original sample depth did not affect P^*_{max} in the incubations for Stations 5, 13, and 35, and there was no interaction between Fe and

Table 4. Physiological characteristics[a] of phytoplankton in the bioassay experiments[b]

Characteristic	Bioassay experiment	Station-specific data by sample type						Station-specific data by light level					
		Station 5		Station 13		Station 35		Station 57			Station 66		
		S	D	S	D	S	D	1%	10%	50%	1%	10%	50%
Phytoplankton growth rate (d^{-1})	C	0.26 (0.01)	0.31 (0.01)	0.25 (0.01)	0.24 (0.02)	0.10 (0.01)	0.12 (0.01)	0.06 (0.01)	0.29 (0.00)	0.28 (0.01)	0.07 (0.01)	0.18 (0.01)	0.19 (0.01)
	Fe	0.29* (0.00)	0.33 (0.01)	0.24 (0.01)	0.30 (0.00)	0.19 (0.01)	0.26* (0.01)	0.08 (0.01)	0.31* (0.00)	0.33 (0.00)	0.06 (0.02)	0.23 (0.01)	0.19 (0.01)
POC/Chl a (wt/wt)	C	58 (5)	102 (17)	73 (20)	89 (17)	75 (2)	56 (12)	36 (3)	60 (10)	89 (9)	65 (7)	79 (5)	108 (7)
	Fe	72 (14)	84 (15)	229 (212)	67 (19)	75 (19)	79 (15)	44 (3)	64 (7)	101 (26)	73 (10)	116* (15)	131 (29)
POC/PON (mol/mol)	C	5.1 (1.5)	5.4 (0.5)	7.3 (0.6)	6.8 (0.2)	6.3 (0.2)	6.2 (0.3)	6.3 (3.5)	6.6 (0.2)	4.9 (1.3)	5.6 (0.4)	5.8 (0.6)	4.6 (0.3)
	Fe	4.0 (0.7)	5.1 (1.0)	6.8 (1.1)	6.5 (0.2)	8.5 (1.9)	6.5 (0.5)	4.6 (0.3)	5.4 (0.8)	5.1 (1.1)	6.2 (1.1)	6.6 (0.6)	5.4 (1.1)
$\bar{a}^*$ (photons m^{-2})	C	0.014	0.016	0.014	0.017	0.015	0.013	0.010	0.012	0.014	0.011	0.012	0.012
	Fe	0.015	0.015	0.016	0.013	0.011	0.009	0.014	0.012	0.011	ND	0.013	0.013
Φ^m (mol C mol^{-1} photons)	C	0.076	0.102	0.051	0.051	0.066	0.061	0.134	0.100	0.056	0.120	0.080	0.044
	Fe	0.139	0.119	0.073	0.081	0.150	0.173	0.144	0.099	0.137	ND	0.093	0.096

[a] Mean (standard deviation) by day 4; asterisk indicates significant effect of Fe addition (one-way ANOVA, $p < 0.05$)
[b] Abbreviations (and units): S = surface water sample, D = deeper subsurface sample, % = level of incident irradiance, C = unamended control, Fe = Fe addition, Chl *a* = Chlorophyll *a* (μg L^{-1}), POC = particulate organic carbon (μg L^{-1}), PON = particulate organic nitrogen, $\bar{a}^*$ = spectrally averaged Chl *a*-specific optical absorption cross section, Φ_m = quantum yield of photosynthesis

doi: 10.12952/journal.elementa.000043.t004

Table 5. Significance of effects[a] of Fe addition, sample depth, and light levels on phytoplankton variables[b] and bacterial productivity

Variable	*p* values[a] for bioassay test (number of experiments)				
	Fe (5)	Depth (3)	Fe x Depth (3)	Light (2)	Fe x Light (2)
Phytoplankton growth rate	0.018*	0.009*	0.668	0.000*	0.723
NO_3 drawdown	0.037*	0.034*	0.202	0.000*	0.280
F_v/F_m	0.008*	0.164	0.866	0.012*	0.093
σ_{PSII}	0.471	0.087	0.665	0.617	0.017*
P^*_{max}	0.039*	0.500	0.527	0.217	0.868
α^*	0.006*	0.851	0.473	0.024*	0.322
E_k	0.419	0.359	0.701	0.000*	0.002*
$\bar{a}^*$	0.234	0.379	0.219	0.381	0.822
Φ_m	0.005*	0.796	0.935	0.005*	0.051
POC/PON	0.977	0.665	0.731	0.119	0.586
POC/Chl *a*	0.124	0.440	0.170	0.000*	0.785
Bacterial productivity	0.311	0.928	0.533	0.618	0.951

[a]Measured at day 4 of the experiment; *p* values are for two-way ANOVA analysis of the bioassay experiments analyzed together; asterisk indicates significant effect at the $p < 0.05$ level.
[b]Variables: F_v/F_m = maximum photochemical efficiency of photosystem II, σ_{PSII} = functional absorption cross section, P^*_{max} = maximum rate of photosynthesis, α^* = initial slope of photosynthesis versus irradiance curve, E_k = photoacclimation parameter, Φ_m = quantum yield of photosynthesis, $\bar{a}^*$ = spectrally averaged Chl *a*-specific optical absorption cross section, POC = particulate organic carbon, PON = particulate organic nitrogen.

doi: 10.12952/journal.elementa.000043.t005

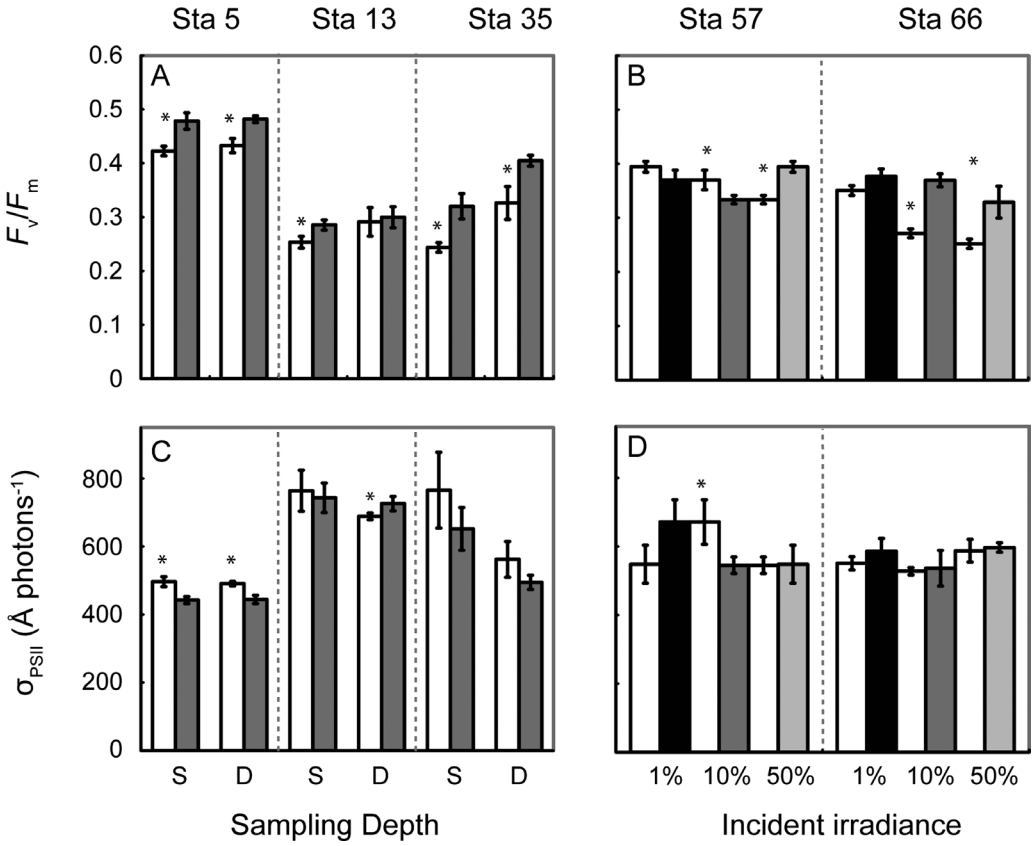

Figure 7

Variable fluorescence in incubation experiments.

Mean and standard deviation of variable fluorescence by day 4 of the incubation experiments are shown for triplicate incubations of Fe additions (dark bars) and unamended controls (white bars). An asterisk indicates significant difference between Fe addition and control (one-way ANOVA, $p<0.05$). Maximum photochemical efficiency of Photosystem (PS) II (F_v/F_m) is shown for surface (S) and deeper subsurface (D) incubations from Stations 5, 13 and 35 (A) and for different levels of incident irradiance (1%, black; 10%, grey; 50%, light grey) for Stations 57 and 66 (B). Functional cross section of PS II (σ_{PSII}) is shown for the surface and subsurface depths (C) and levels of incident irradiance (D).

doi: 10.12952/journal.elementa.000043.f007

depth (Table 5). P^*_{max} increased slightly with higher light, although this effect was not significant; there was no interaction between Fe and light effects (Table 5).

The α^* was high in all incubations (> 0.024 µg C µg^{-1} Chl *a* h^{-1} [µmol photons m^{-2} s^{-1}]$^{-1}$, Figures 8C, 8D) and generally followed the trends in P^*_{max}. Fe addition increased α^* in almost all experiments (Figures 8C, 8D), on average by 1.42-fold. This increase was greatest in the incubations where Fe additions also affected phytoplankton growth (S for Station 5, D for Station 35), where α^* increased 1.89-fold and 1.95-fold, respectively. Thus, in Fe-limited phytoplankton, the relative effect of Fe on α^* was greater than that on P^*_{max}. When all experiments were analyzed together, the Fe effect on α^* was significant (Table 5). The original sample depth did not affect α^* in the incubations at Stations 5, 13, and 35, and there was no interaction between Fe and sample depth (Table 5). The α^* decreased at higher light, but there was no interaction between Fe and light effects (Table 5).

The photoacclimation parameter (E_k) was high (53–104 µmol photons m^{-2} s^{-1}) in all incubations at 10% and 50% irradiance and somewhat lower at 1% irradiance (42–46 µmol photons m^{-2} s^{-1}) (Figures 8E, 8F). Fe addition did not affect E_k because both α^* and P^*_{max} increased relative to the controls. When all experiments were analyzed together, E_k was not significantly affected by either Fe, depth, or the interaction between Fe and depth (Table 5). On the other hand, E_k increased at higher light and there was an interaction between Fe and light effects (Table 5), where Fe addition at high light (50% irradiance) decreased E_k, but there was no effect at lower light.

The $\overline{a}^*$ in the incubations varied between 0.009 and 0.017 m^{-2} mg^{-1} Chl *a* (Table 4) and was similar to initial $\overline{a}^*$ of phytoplankton in the ASP (Table 2B). Fe addition did not affect $\overline{a}^*$ in any of the incubations (Table 4). Moreover, when experiments were analyzed together, there was no effect of either Fe, sample depth, or light on $\overline{a}^*$, and there were no interactive effects (Table 5).

The Φ_m in the incubations varied between 0.051 and 0.173 mol C mol^{-1} photons (Table 4) and was similar to initial Φ_m of phytoplankton in the ASP (Table 2B). Fe addition increased Φ_m in all incubations, on average 1.51-fold (Table 4, Table 5). There was no effect of original sample depth on the Φ_m in the incubations and there were no interactions between Fe and depth effects (Table 5). The Φ_m was higher at low light (Table 4, Table 5) and there was an interaction between Fe and light effects (Table 5), where the Fe effect was stronger at high light.

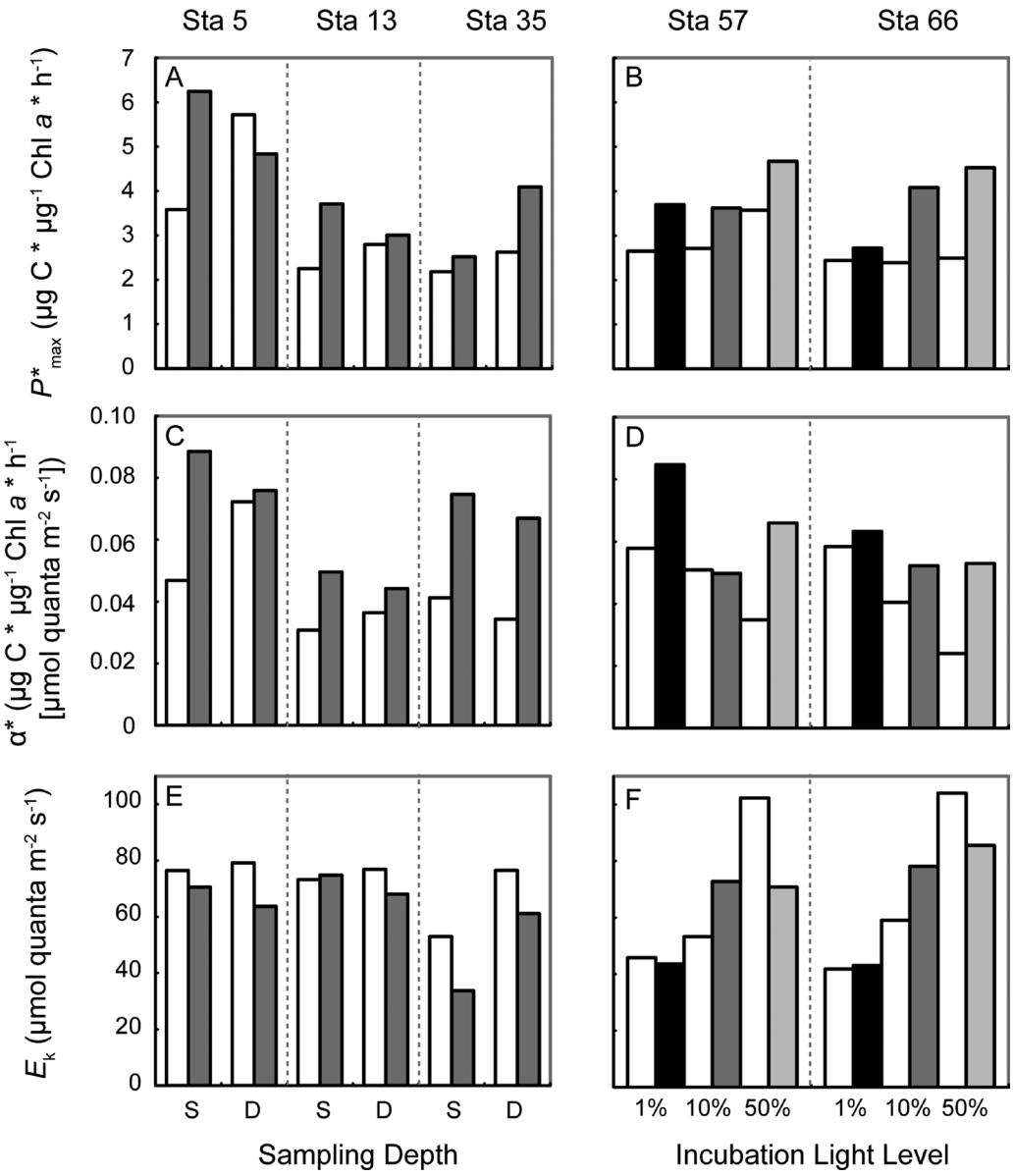

Figure 8

Photosynthesis versus irradiance parameters in incubation experiments.

Photosynthesis versus irradiance (*P-E*) parameters at day 4 of the incubation experiments are shown for incubations of Fe additions (dark bars) and unamended controls (white bars). Maximum photosynthesis rates (P^*_{max}) are shown for surface (S) and deeper subsurface (D) incubations from Stations 5, 13 and 35 (A) and for different levels of incident irradiance (1%, black; 10%, grey; 50%, light grey) for Stations 57 and 66 (B). Initial slope of the *P-E* curve (α^*) is shown for the surface and subsurface depths (C) and levels of incident irradiance (D), as is photoacclimation parameter (E_k) (E & F).

doi: 10.12952/journal.elementa.000043.f008

Cellular composition of phytoplankton

The POC/PON ratios in the incubations showed considerable variation by day 4, ranging from 3.5 to 8.5 (Table 4). The highest POC/PON ratio was found in the Fe incubations of surface waters from Station 35 that were NO_3-limited. Fe addition did not affect the POC/PON ratio in any of the experiments (Table 4), and the lack of Fe effect was confirmed when experiments were analyzed together (Table 5).

The POC/Chl *a* ratios in the incubations ranged from 36 to 229 g g^{-1} (Table 4). Fe addition increased the POC/Chl *a* ratio in the 10% irradiance incubation at Station 66, but did not affect the POC/Chl *a* ratio in any other incubations (Table 4). When all experiments were analyzed together, Fe additions enhanced POC/Chl *a* ratios slightly (1.14-fold) compared to the controls, but this difference was not significant (Table 5). Initial sampling depth did not affect POC/Chl *a* ratios in the incubations, and there was no interaction between depth and Fe effects (Table 5). On the other hand, the POC/Chl *a* decreased at low light incubations, but there was no interaction between Fe and light effects on POC/Chl *a* (Table 5).

Bacterial productivity

Bacterial productivity in the incubations by day 4 ranged from 36 to 289 pmol Leu uptake L^{-1} h^{-1} (Figure 9). It increased 2 to 17-fold over the course of 4 days in all incubations, except for Station 57 at 1% irradiance, where bacterial productivity dropped slightly from the initial value (compare Figure 9 to Table 2B). Fe addition did not affect bacterial productivity in any of the incubations (Figure 9), including the incubations where Fe addition

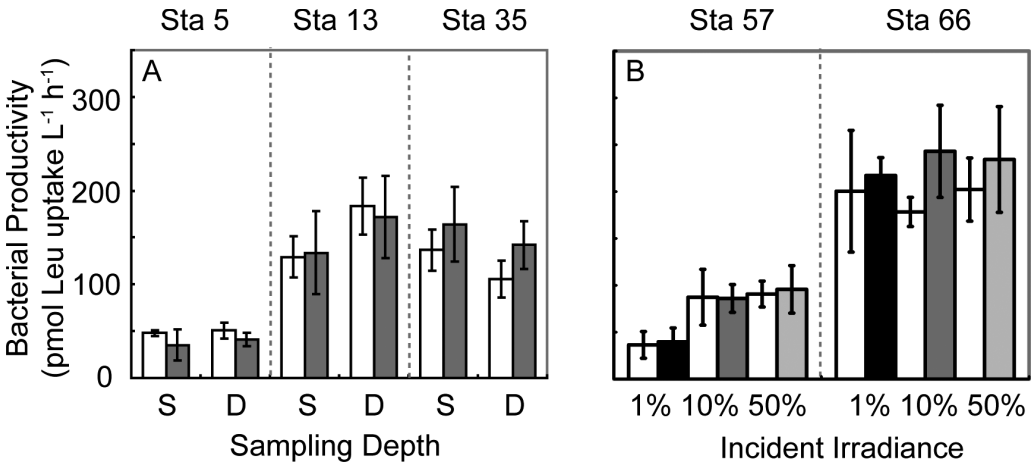

Figure 9

Bacterial productivity in incubation experiments.

Mean and standard deviation of bacterial productivity by day 4 of the incubation experiments are shown for triplicate incubations of Fe additions (dark bars) and unamended controls (white bars). Rates are shown for surface (S) and deeper subsurface (D) incubations from Stations 5, 13, and 35 (A) and for different levels of incident irradiance (1%, black; 10%, grey; 50%, light grey) for Stations 57 and 66 (B).

doi: 10.12952/journal.elementa.000043.f009

enhanced phytoplankton growth (Station 5, S; Station 35, D; Station 57, 10%), suggesting that there were no secondary effects of bacterial productivity on Fe-enhanced phytoplankton growth and photosynthesis. Moreover, original sample depth did not significantly affect bacterial productivity in the incubations, and there was no interaction between Fe and depth effects (Table 5). Light levels in the incubations did not affect bacterial productivity either, despite the big difference in phytoplankton biomass between the 1% irradiance incubations and those at higher light (10% and 50% irradiance) (Table 5).

Discussion

Phytoplankton response to Fe additions: carrying capacity versus rate limitation

Phytoplankton productivity in Antarctic polynyas is often assumed to be seasonally Fe limited, with a "winter reserve" of DFe that is gradually depleted over the growing season. The amount of phytoplankton biomass that is supported by this DFe has been referred to as the carrying capacity (Hopkinson et al., 2013). Since all available NO_3 was drawn down in both the controls and Fe addition incubation experiments with sufficient light (the 10% and 50% light incubations), the results from the incubation experiments suggest that Fe availability is not limiting the carrying capacity of waters in the ASP. Moreover, previous bioassay experiments conducted later in the growing season showed no response of the phytoplankton biomass to Fe additions in the ASP in February 2009 (Mills et al., 2012). These experiments were performed after the peak in phytoplankton bloom for that season, suggesting that Fe limitation was not the cause of the bloom demise.

In contrast, Fe addition increased phytoplankton growth rates at several stations where we performed bioassay experiments (Station 5, surface water; Station 35, subsurface water; Station 57, 10% light; Figure 6; Table 4) during the build-up of the phytoplankton spring bloom, and enhanced photosynthesis rates in almost all experiments (Figure 8). Thus, even though Fe availability is not limiting the carrying capacity of the ASP (Mills et al., 2012), the Fe effects in the bioassay experiments suggest that Fe availability may limit phytoplankton growth rates in several regions of the ASP. We could not discern physical mechanisms (e.g., MLD, water mass properties) that could explain the spatial variability of Fe effects on phytoplankton growth. The timing of the Fe effects in mid-December to early January was early in the growing season, well before the peak of the phytoplankton bloom in the ASP, which is generally in the middle of January (Arrigo et al., 2012). These findings suggest that the notion of a "winter reserve" of DFe that is gradually depleted over the growing season is an oversimplification, concurring with findings by Sedwick et al. (2011) who showed early season depletion of DFe in the Ross Sea Polynya. Instead, bioavailable Fe must be supplied throughout the growing season to support productive phytoplankton blooms such as those observed in the Amundsen and Ross Sea Polynyas.

Bacterial productivity in the incubation experiments was similar to that reported in the high productivity stations in the central ASP, which was high compared to other Antarctic polynyas (see Williams et al., 2015, for a full description). In contrast to phytoplankton growth and photosynthesis, bacterial productivity did not respond to Fe addition, suggesting that bacteria are not Fe-limited during the early season in the ASP. The Fe demand of bacteria is generally lower than that of phytoplankton, as heterotrophic bacteria lack the photosynthetic apparatus that is rich in Fe (Raven et al., 1990). Moreover, bacteria are smaller, with a larger surface to volume ratio that optimizes nutrient uptake. In addition, despite the increase in bacterial productivity over the four days of incubation, there was no secondary response of bacterial productivity to either the Fe-enhanced phytoplankton growth or photosynthesis rates. Bacterial productivity in surface waters of the ASP showed a positive relationship with phytoplankton biomass (Williams et al., 2015), suggesting

bacterial productivity was coupled to phytoplankton biomass and productivity. Likely, the Fe effects on phytoplankton biomass, cellular composition, and photosynthesis rates in our experiments were not sufficient to yield a detectable response in bacterial productivity during the time scale of the incubations.

Fe availability as the main driver for phytoplankton photosynthesis rates in the ASP

The Fe addition bioassay experiments showed that greater Fe availability increased all photosynthesis parameters, including F_v/F_m, P^*_{max}, and α^*, similar to results from culture experiments on *Phaeocystis antarctica* (Strzepek et al., 2012; Alderkamp et al., 2012b; Van Leeuwe and Stefels, 2007). On the other hand, increased light availability in the bioassay experiments increased P^*_{max}, but decreased α^* and F_v/F_m. Typically, photoacclimation to high light increases carbon-fixing activity, such as electron transport and the Calvin cycle, resulting in a higher cellular C/Chl *a* ratio, whereas it decreases the photon capture and photosynthetic efficiency at low light (Falkowski and LaRoche, 1991; MacIntyre et al., 2002). The spatial distribution of *P-E* parameters of surface phytoplankton (upper 10 m) in the ASP showed a positive relationship between F_v/F_m, P^*_{max}, and α^*, indicating that phytoplankton acclimation to Fe availability, rather than light availability, is the main driver of photosynthesis rates in the ASP during the build-up of the phytoplankton bloom.

Surface phytoplankton F_v/F_m, P^*_{max}, as well as α^*, were highest in the southern ASP near the ice shelves (Stations 5 and 57), suggesting that the WW near the GIS, as well as meltwater-laden mCDW from the DIS, are major Fe sources to phytoplankton. On the other hand, F_v/F_m, P^*_{max} and α^* were all lower in the central polynya, suggesting that Fe availability limited photosynthesis rates where the phytoplankton biomass was highest. The F_v/F_m, P^*_{max} and α^* in the low salinity AASW strongly affected by recent sea ice melt (Stations 34 and 66) were intermediate, suggesting that melting sea ice may be an Fe source (Sedwick and DiTullio, 1997; Lannuzel et al., 2010), albeit not as pronounced as the ice shelves. The P^*_{max} at Stations 5 and 57 close to the ice shelves (3.6 g C g^{-1} Chl *a* h^{-1}) was 1.6-fold higher than in the central polynya (2.2 g C g^{-1} Chl *a* h^{-1}), whereas α^* close to the ice shelves (0.067 g C g^{-1} Chl *a* h^{-1} [µmol photons m^{-2} s^{-1}]$^{-1}$) was 1.9-fold higher than in the central polynya (0.035 g C g^{-1} Chl *a* h^{-1} [µmol photons m^{-2} s^{-1}]$^{-1}$). Both P^*_{max} and α^* close to the ice shelves exceeded values in the controls of the bioassay experiments, and matched those of the Fe treatments, as well as those in *P. antarctica* cultures growing under Fe-replete and saturating light conditions (Arrigo et al., 2010; Mills et al., 2010).

Curiously, there was no direct relationship between DFe concentrations in surface waters and any *P-E* parameter. High P^*_{max} (> 3 g C g^{-1} Chl *a* h^{-1}) and high α^* (> 0.05 g C g^{-1} Chl *a* h^{-1} [µmol photons m^{-2} s^{-1}]$^{-1}$) were observed in waters with DFe as low as 0.11 nmol L^{-1}. Similarly, DFe concentrations in the initial waters of the bioassay experiments did not alter the effects of Fe addition on phytoplankton growth. For instance, Fe addition did not affect phytoplankton growth in waters with the lowest initial DFe in this study (surface waters of Station 13, 0.09 nmol L^{-1} DFe), whereas initial DFe in the incubations that did show an Fe effect (Station 5 surface water, Station 35 subsurface water) were approximately twice as high at 0.18 and 0.22 nmol L^{-1} DFe, respectively. Thus, DFe concentrations do not appear to be a good measure of Fe availability for phytoplankton. A lack of direct DFe effects on phytoplankton photosynthesis and growth suggests that either not all DFe was bioavailable to the phytoplankton (Visser et al., 2003) or other sources of bioavailable Fe were present besides DFe (e.g., PFe). In addition, phytoplankton cells may have stored bioavailable DFe in excess of their immediate needs, resulting in Fe-replete cells in Fe-depleted waters.

Bioavailability of at least a fraction of PFe is suggested by the positive relationship between PFe and both P^*_{max} and α^*, indicating that PFe contributes to the pool of bioavailable Fe, or becomes bioavailable at high enough rates to support high photosynthesis rates. A small fraction of this PFe may be internal or attached to phytoplankton cells (Twining and Baines, 2013). Several studies show that Fe:C ratios of Fe-replete phytoplankton are a factor of 2 to 10 higher than those of Fe-limited phytoplankton (Twining et al., 2004; Hassler and Schoemann, 2009; Strzepek et al., 2012), suggesting that phytoplankton have the ability to take up DFe in excess of their immediate requirements and store it. Studies with *P. antarctica* suggest that metals may be stored inside *P. antarctica* colonies (Lubbers et al., 1990; Schoemann et al., 2001). The fraction of PFe internal or attached to cells is likely small, given that the highest PFe was observed at the face of the DIS where phytoplankton biomass was low.

Alternatively, extracellular, inorganic PFe in the ASP, such as crustal particles and Fe hydroxides (Hazarin et al., 2014), may be made biologically available through dissolution, photoreduction, and/or biological processing (Barbeau et al., 2003; Boyd and Ellwood, 2010; Rijkenberg et al., 2006, 2008; Boyd and Ellwood, 2010). Since E_{UML} was relatively high throughout the ASP (Figure 3D), photoreduction is likely an active process in surface waters of the ASP. Photoreduction can convert bound Fe(III) species to Fe(II) via ligand to metal charge transfer (Barbeau et al., 2003; Rijkenberg et al., 2006). The *P. antarctica* bloom is associated with an abundance of relatively unsaturated organic Fe-binding ligands (Thuróczy et al., 2012) that may bind the Fe (II), keep it in solution (Rijkenberg et al., 2006, 2008), and make it available to *P. antarctica*. Specifically, polysaccharides enhance Fe bioavailability to both *P. antarctica* and diatoms (Hassler et al., 2011); as the main constituent of the matrix of *Phaeocystis* colonies (Alderkamp et al., 2007), polysaccharides may thus make PFe available to *P. antarctica*.

Effects of Fe limitation on phytoplankton photosynthesis at different light intensities

Phytoplankton acclimation to low Fe availability in the ASP will affect their photophysiology because of the high Fe requirements for chlorophyll biosynthesis and the high Fe content of the photosynthetic apparatus and electron transport pathways (Raven, 1990; Maldonado et al., 1999; Strzepek and Price, 2000). In general, acclimation to low Fe decreases the potential to maximize photon capture (Raven, 1990; Greene et al., 1992). Despite this interaction, the incubation experiments showed no interactive effects of Fe and light availability on photosynthesis rates. Two possible reasons for this lack of interaction may be that Antarctic phytoplankton do not increase their Fe quota to photoacclimate to low light (Strzepek et al., 2012), or that light-limited phytoplankton have lower growth rates and therefore require less Fe per unit time, i.e., a lower Fe flux.

For the first explanation for the lack of interaction between Fe and light availability on phytoplankton photosynthesis in the bioassay experiments, we consider photoacclimation strategies. Photoacclimation to low light may be achieved by either increasing the number of PSII reaction centers (RCIIs) or increasing the size of the photosynthetic pigment-containing antenna associated with the RCIIs; both strategies increase the cellular photosynthetic pigment concentrations. Increasing the number of RCIIs, however, increases the Fe requirement because the RCII and downstream electron transport chain are particularly Fe-rich: photosystem II (PSII) contains two or three Fe atoms, the cytochrome b_6f complex (Cyt b_6f) contains five Fe atoms, and PSI contains 12 Fe atoms (Raven, 1990). The σ_{PSII} is the functional absorption cross section of PSII and can be used to distinguish between the two different photoacclimation strategies. The σ_{PSII} is the product of absorption by the PSII antenna pigments and the probability that an exciton within the antenna will cause a photochemical reaction (Mauzerall and Greenbaum, 1989). The amount of pigment associated with each RCII will therefore determine much of the variability in σ_{PSII} (Kolber et al., 1988; Suggett et al., 2004). Acclimation responses that alter the ratio of pigment:RCII will change the σ_{PSII}, whereas acclimation responses that alter the number of RCIIs per cell but not the amount of pigments associated with it will not affect the σ_{PSII} (Moore et al., 2006).

Light availability did not affect σ_{PSII} in either the incubation experiments (Figure 7D) or the water column (Figure 5C), suggesting that the *P. antarctica*–dominated phytoplankton community did not change its antenna size during photoacclimation to low light, but rather increased the number of RCIIs, which would increase the cellular Fe requirement, contradicting the notion that Antarctic phytoplankton do not increase their Fe quota at low light (Strzepek et al. 2012). Our results match field results of σ_{PSII} from the Ross Sea, where σ_{PSII} did not increase with depth at *P. antarctica*–dominated stations (Smith et al., 2013). In contrast, *P. antarctica* did increase σ_{PSII} under lower growth irradiance in culture experiments (Strzepek et al., 2012). Whether different strains of *P. antarctica* vary in their ability to adjust σ_{PSII} or the timescales of photoacclimation in the field are too long to observe changes in σ_{PSII} during four-day incubation is unknown.

Similar to light availability, Fe availability did not affect σ_{PSII} consistently when control and Fe treatments were compared in the bioassay experiments. Moreover, there was no spatial pattern in σ_{PSII} of surface phytoplankton in the ASP, despite the low Fe availability in the central ASP. These observations suggest that *P. antarctica* in the ASP does not increase its antenna size under Fe limitation. These results contrast with the increase in σ_{PSII} under Fe limitation reported in culture experiments, where the σ_{PSII} of Fe-limited *P. antarctica* was two-fold higher than Fe-replete *P. antarctica* under similar growth irradiance (Strzepek et al., 2012). The maximum response of σ_{PSII} to Fe limitation in our incubation experiments was more subtle, with a 1.23-fold increase in control versus Fe treatments. Again, these differences between field observations and culture experiments could be due to (unknown) variability among different strains of *P. antarctica* in their ability to adjust σ_{PSII}, or to timescales of acclimation.

The second explanation for the lack of interactions between Fe and light availability on phytoplankton photosynthesis rates is that light-limited phytoplankton have lower growth rates and therefore require less Fe per unit time. For our incubation experiments, this reduced requirement would mean that there was enough DFe in the original waters sampled to support slow-growing phytoplankton until day four of the incubation, but not enough to support fast-growing phytoplankton. In the field, if the DFe supply to a phytoplankton bloom is considered in terms of Fe flux, light-limited phytoplankton with low growth rates would require a lower Fe flux than phytoplankton with high growth rates under high light. Thus, if the DFe flux remains constant, phytoplankton under high light availability, as in the central ASP, may experience more Fe stress than light-limited phytoplankton that are growing more slowly, even if high light phytoplankton would have a lower Fe quota.

Water column productivity in the ASP driven by both Fe and light

Despite Fe limitation of photosynthesis rates, phytoplankton biomass and water column productivity was high throughout the ASP (2.1–6.5 g C m^{-2} d^{-1}). These rates were similar to primary productivity rates reported by Lee et al. (2012) and Yager et al. (2014) during the same period in the ASP, and similar to rates measured later in the season in a previous year (Alderkamp et al., 2012a). Moreover, the high phytoplankton biomass and productivity match the high primary productivity rates calculated from satellite data in the ASP (Arrigo and

Van Dijken, 2003; Arrigo et al., 2012; Yager et al., 2012). In addition, these high water column productivity rates were similar to those in the Pine Island Polynya in the eastern Amundsen Sea (Alderkamp et al., 2012a).

Stations with the highest water column productivity were all located in the moderately fresh AASW layer in the central ASP, where sea ice melt signatures were found enhancing stratification (MLD < 30 m) and increasing light availability. Although we could not find any direct relationship between water column productivity and parameters affecting light availability, such as MLD and E_{UML}, autonomous glider observations at high spatial resolution within the central ASP found a positive relationship between phytoplankton biomass and enhanced stratification (shallower MLD) (Schofield et al., 2015), suggesting an important role for light availability in bloom formation. Stratification, resulting in enhanced light availability to phytoplankton, is especially important for bloom development early in the season (i.e., October–November) (Long et al., 2012), when incident irradiance is relatively low due to lower solar elevation and shorter days compared to the sampling period of this study (i.e. December–January).

The high water column productivity in the central ASP coincided with the stations where P^*_{max} and α^* were limited by Fe availability. In order to estimate the effect of Fe-replete photosynthetic parameters on water column productivity in the central ASP, we used the enhanced *P-E* parameters close to the ice shelves (Stations 5 and 57) for water column productivity calculations in the central polynya. This calculation showed that enhanced *P-E* parameters under high Fe availability have the potential to increase water column productivity in the central polynya on average by 1.7 ±0.01-fold, assuming all other factors stay the same (e.g., light availability, temperature, grazing, phytoplankton species composition). Thus, increased Fe availability during the build-up of the bloom would significantly increase the already high rates of phytoplankton productivity in the ASP.

Many Antarctic ice shelves are thinning, including the Dotson Ice Shelf, as the glaciers that feed these ice shelves are accelerating (Pritchard et al., 2009; Rignot et al., 2013). An increase in basal ice shelf melt would most likely be driven by an increase in the amount of mCDW flowing onto the continental shelf and/or an increase in the heat content of mCDW (Jacobs et al., 2011). An increase in meltwater-laden mCDW exiting the ice shelve cavities would destabilize the water column, potentially increasing MLD and decreasing light availability. Early in the growing season when incident irradiance is relatively low, this scenario would potentially delay bloom formation and decrease water column productivity, especially near the ice shelf. However, if the DIS is a source of bioavailable Fe for the ASP, similar to that observed for the Pine Island ice shelf in the PIP (Gerringa et al., 2012), then horizontal diffusivity (Geringa et al., 2012), advective eddy transport (e.g., Årthun et al., 2013), mixing along the Dotson trough (e.g., St-Laurent et al., 2013), and wind- and iceberg-induced mixing (Randall-Goodwin et al., 2015) would ensure a bioavailable Fe flux from the DIS or neighboring ice shelves to the high phytoplankton biomass in the central ASP, where the water column is stabilized by sea ice melt water and higher Fe availability would increase the phytoplankton photosynthesis and water column productivity substantially.

The presence of mCDW has been detected regularly in the troughs of the ASP since observations began (Jacobs et al., 2012; Arneborg et al., 2012; Wåhlin et al., 2013; Ha et al., 2014), suggesting this water mass has regular access to the DIS. However, any seasonal (Thoma et al., 2008; Jacobs et al., 2012; Randall-Goodwin et al., 2015) or annual (Jacobs et al., 2013; Dutrieux et al., 2014) variability in mCDW on the continental shelf will likewise affect the quantity of meltwater-laden mCDW from the DIS, and hence the DFe flux to the ASP. Variability in the DFe flux would affect phytoplankton photosynthetic rates directly according to our results. How phytoplankton productivity across the ASP would be affected by variability in mCDW access to the DIS is unknown, but represents a key question for future investigations.

References

Ainley DG, Ballard G, Dugger KM. 2006. Competition among penguins and cetaceans reveals trophic cascades in the western Ross Sea, Antarctica. *Ecology* **87**: 2080–2093.

Alderkamp A-C, Buma AGJ, Van Rijssel M. 2007. The carbohydrates of *Phaeocystis* and their degradation in the microbial food web. *Biogeochemistry* **83**: 99–118.

Alderkamp A-C, Kulk G, Buma AGJ, Visser RJW, Van Dijken GL, et al. 2012b. The effect of iron limitation on the photophysiology of *Phaeocystis antarctica* (Prymnesiophyceae) and *Fragilariopsis cylindrus* (Bacillariophyceae) under dynamic irradiance. *J Phycol* **48**: 45–59. doi: 10.1111/j.1529-8817.2011.01098.x.

Alderkamp A-C, Mills MM, Van Dijken GL, Laan P, Thuyróczy C-E, et al. 2012a. Iron from melting glaciers fuels phytoplankton blooms in the Amundsen Sea (Southern Ocean): Phytoplankton characteristics and productivity. *Deep-Sea Res Pt II* **71–76**: 32–48. doi: 10.1016/j.dsr2.2012.03.005.

Arneborg L, Wåhlin AK, Björk G, Liljebladh B, Orsi AH. 2012. Persistent inflow of warm water onto the central Amundsen shelf. *Nature Geosciences* **5**: 876–880. doi: 10.1038/NGEO1644.

Arrigo KR, Lowry KE, Van Dijken GL. 2012. Annual changes in sea ice and phytoplankton in polynyas of the Amundsen Sea, Antarctica. *Deep-Sea Res Pt II* **71–76**: 5–15.

Arrigo KR, Mills MM, Kropuenske LR, Van Dijken GL, Alderkamp A-C, et al. 2010. Photophysiology in two major Southern Ocean taxa: photosynthesis and growth of *Phaeocystis antarctica* and *Fragilariopsis cylindrus* under different irradiance levels. *Integrative Comp Biol* **50**: 950–966.

Arrigo KR, Van Dijken GL. 2003. Phytoplankton dynamics within 37 Antarctic coastal polynya systems. *J Geophys Res-Oceans* **108**(C8): 3271. doi: 10.1029/2002JC001739.

Arrigo KR, Van Dijken GL, Long MC. 2008. Coastal Southern Ocean: A strong anthropogenic CO_2 sink. *Geophys Res Lett* **35**: L21602. doi: 10.1029/2008GL035624.

Arrigo KR, Worthen DL, Robinson DH. 2003. A coupled ocean-ecosystem model of the Ross Sea: 2. Iron regulation of phytoplankton taxonomic variability and primary production. *J Geophys Res-Oceans* **108**: 3231. doi:10.1029/2001JC000856.

Årthun M, Holland PR, Nicholls KW, Feltham DL. 2013. Eddy-driven exchange between the open ocean and a sub-ice shelf cavity. *J Phys Oceanogr* **43**: 2372–2387.

Barbeau K, Rue EL, Trick CG, Bruland KW, Butler A. 2003. Photochemical reactivity of siderophores produced by marine heterotrophic bacteria and cyanobacteria based on characteristic Fe(III) binding groups. *Limnol Oceanogr* **48**: 1069–1078.

Boyd PW, Ellwood MJ. 2010. The biogeochemical cycle of iron in the ocean. *Nature Geosciences* **3**: 675–682.

Boyd PW, Jickells T, Law CS, Blain S, Boyle EA, et al. 2007. Mesoscale iron enrichment experiments 1993–2005: Synthesis and future directions. *Science* **315**: 612–617.

Bricaud A, Stramski D. 1990. Spectral absorption-coefficients of living phytoplankton and nonalgal biogenous matter - A comparison between the Peru upwelling area and the Sargasso Sea. *Limnol Oceanogr* **35**: 562–582.

Buma AGJ, De Baar HJW, Nolting RF, Van Bennekom AJ. 1991. Metal enrichment experiments in the Weddell-Scotia Seas - Effects of iron and manganese on various plankton communities. *Limnol Oceanogr* **36**: 1865–1878.

Cisewski B, Strass VH, Losch M, Prandke H. 2008. Mixed layer analysis of a mesoscale eddy in the Antarctic Polar Front Zone. *J Geophys Res-Oceans* **113**: C05017. doi: 10.1029/2007JC004372.

De Baar HJW, Boyd PW, Coale KH, Landry MR, Tsuda A, et al. 2005. Synthesis of iron fertilization experiments: From the iron age in the age of enlightenment. *J Geophys Res-Oceans* **110**: C09S16.

De Jong J, Schoemann V, Mairq N, Mattielli N, Langhorne P, et al. 2013. Iron in land-fast sea ice of McMurdo Sound derived from sediment resuspension and wind-blown dust attributes to primary productivity in the Ross Sea, Antarctica. *Mar Chem* **157**: 24–40. doi: 10.1016/j.marchem.2013.07.001.

DiTullio GR, Garcia N, Riseman SF, Sedwick PN. 2007. Effects of iron concentration on pigment composition in *Phaeocystis antarctica* grown at low irradiance. *Biogeochemistry* **83**: 71–78.

Dutrieux P, De Rydt J, Jenkins A, Holland PR, Ha HK, et al. 2014. Strong sensitivity of Pine Island ice-shelf melting to climatic variability. *Science* **343**: 174–178. doi: 10.1126/science.1244341.

Falkowski PG, LaRoche J. 1991. Acclimation to spectral irradiance in algae. *J Phycol* **27**: 8–14.

Gerringa LJA, Alderkamp A-C, Laan P, Thuróczy C-E, De Baar HJW, et al. 2012. Iron from melting glaciers fuels the phytoplankton blooms in Amundsen Sea (Southern Ocean); iron biogechemistry. *Deep-Sea Res Pt II* **71–76**: 16–31.

Gorbunov MY, Kolber ZS, Falkowski PG. 1999. Measuring photosynthetic parameters in individual algal cells by Fast Repetition Rate fluorometry. *Photosynth Res* **2**: 141–153.

Greene RM, Geider RJ, Kolber ZS Falkowski PG. 1992. Iron-induced changes in light harvesting and photochemical energy-conversion processes in eukaryotic marine-algae. *Plant Physiol* **100**: 565–575.

Ha HK, Wåhlin AK, Kim TW, Lee JH, Lee HJ, et al. 2014. Circulation and modification of warm deep water on the central Amundsen shelf. *J Phys Oceanogr* **44**: 1493–1501.

Harazin KM, Lagerström M, Forsch KO, Severmann S, Sherrell RM. 2014. The metal-to-phosphorous ratio of natural phytoplankton assemblages in the Amundsen Sea Polynya and western Antarctic Peninsula, west Antarctica. 2014. *Ocean Sciences Meeting*. Honolulu, Hawaii.

Hassler CS, Schoemann V. 2009. Bioavailability of organically bound Fe to model phytoplankton of the Southern Ocean. *Biogeosciences* **6**: 2281–2296.

Hassler CS, Scoemann V, Nichols CM, Butler ECV, Boyd PW. 2011. Saccharides enhance iron availability to Southern Ocean phytoplankton. *P Natl Acad Sci USA* **108**: 1076–1081.

Hatta M, Measures CI, Selph KE, Zhou M, Hiscock WT. 2013. Iron fluxes from the shelf regions near the South Shetland Islands in the Drake Passage during the austral-winter 2006. *Deep-Sea Res Pt II* **90**: 89–101. doi: 10.1016/j.dsr2.2012.11.003.

Holm-Hansen O, Lorenzen C, Holmes RW, Strickland JDH. 1965. Fluorometric determination of chlorophyll in Chlorophyta, Chrysophyta, Phaeophyta, Pyrrophyta. *J Cons Perm Inter Explor Mer* **30**: 3–15.

Hopkinson BN, Seegers B, Hatta M, Measures CI, Mitchell BG, et al. 2013. Planktonic C:Fe ratios and carrying capacity in the southern Drake Passage. *Deep-Sea Res Pt II* **90**: 102–111.

Jacobs SS, Giulivi C, Dutrieux P, Rignot E, Nitsche F, et al. 2013. Getz ice shelf melting response to changes in ocean forcing. *J Geophys Res* **118**: 1–17. doi:10.1002/jgrc.20298.

Jacobs SS, Hellmer HH, Jenkins A. 1996. Antarctic ice sheet melting in the Southeast Pacific. *Geophys Res Lett* **23**: 957–960.

Jacobs SS, Jenkins A, Giulivi CF, Dutrieux P. 2011. Stronger ocean circulation and increasing melting under Pine Island Glacier ice shelf. *Nature Geosciences* **4**: 519–523.

Jacobs SS, Jenkins A, Hellmer HH, Giulivi C, Nitsche F, et al. 2012. The Amundsen Sea and the Antarctic Ice Sheet. *Oceanography* **25**: 154–163. doi: 10.5670/oceanog.2012.90.

Jenkins A, Dutrieux P, Jacobs SS, McPhail SD, Perrett JR, et al. 2010. Observations beneath Pine Island Glacier in West Antarctica and implications for its retreat. *Nature Geoscience* **3**: 468–472.

Johnson Z, Barber RT. 2003. The low-light reduction in the quantum yield of photosynthesis: potential errors and biases when calculating the maximum quantum yield. *Photosynth Res* **75**: 85–95.

Kishino M, Takahashi M, Okami N, Ichimura S. 1985. Estimation of the spectral absorption-coefficients of phytoplankton in the sea. *B Mar Sci* **37**: 634–642.

Klunder M, Laan P, Middag R, De Baar HJW. 2011. Dissolved iron in the Southern Ocean (Atlantic sector). *Deep-Sea Res Pt II* **58**: 2678–2694.

Kolber ZS, Prášil O, Falkowski PG. 1988. Measurements of variable chlorophyll fluorescence using fast repetition rate techniques: defining methodology and experimental protocols. *Biochim Biophys Acta* **1367**: 88–106.

Lannuzel D, Schoemann V, De Jong J, Pasquer B, Van der Merwe P, et al. 2010. Distribution of dissolved iron in Antarctic sea ice: Spatial, seasonal, and inter-annual variability. *J Geophys Res-Biogeosciences* **115**: G03022. doi: 10.1029/2009JG001031.

Lee SH, Kim BK, Yun MS, Joo H, Yang EJ, et al. 2012. Spatial distribution of phytoplankton productivity in the Amundsen Sea, Antarctica. *Polar Biol* **35**: 1721–1733.

Lewis MR, Smith JC. 1983. A small volume, short-incubation-time method for measurement of photosynthesis as a function of incident irradiance. *Mar Ecol-Prog Ser* **13**: 99–102.

Long MC, Thomas LN, Dunbar RB. 2012. Control of phytoplankton bloom inception in the Ross Sea, Antarctica, by Ekman restratification. *Global Biogeochem Cy* **26**: GB1006. doi: 10.1029/2010GB003982.

Lubbers GW, Gieskes WWC, DelCastilho P, Salomons W, Bril J. 1990. Manganese accumulation in the high pH micro-environment of *Phaeocystis*-sp (haptophyceae) colonies from the North-Sea. *Mar Ecol-Prog Ser* **59**: 285–293.

MacIntyre HL, Kana TM, Anning T, Geider RJ. 2002. Photoacclimation of photosynthesis irradiance response curves and photosynthetic pigments in microalgae and cyanobacteria. *J Phycol* **38**: 17–38.

Mackey MD, Mackey DJ, Higgins HW, Wright SW. 1996. CHEMTAX - A program for estimating class abundances from chemical markers: Application to HPLC measurements of phytoplankton. *Mar Ecol-Prog Ser* **144**: 265–283.

Maldonado MT, Boyd PW, Harrison PJ, Price NM. 1999. Co-limitation of phytoplankton growth by light and Fe during winter in the NE subarctic Pacific Ocean. *Deep-Sea Res Pt II* **46**: 2475–2485. doi: 10.1016/S0967-0645(99)00072-7.

Mankoff KD, Jacobs SS, Tulaczyk SM, Stammerjohn SE. 2012. The role of Pine Island Glacier ice shelf basal channels in deep-water upwelling, polynyas and ocean circulation in Pine Island Bay, Antarctica. *Ann Glaciol* **53**: 123–128, doi:10.3189/2012AoG60A062.

Marsay CM, Sedwick PN, Dinniman MS, Barrett PM, Mack SL, et al. 2014. Estimating the benthic efflux of dissolved iron on the Ross Sea continental shelf. *Geophys Res Lett* **41**: 7576–7583. doi: 10.1002/2014GL061684.

Mauzerall D, Greenbaum NL. 1989. The absolute size of a photosynthetic unit. *Biochim Biophys Acta* **974**: 119–140.

Mills MM, Alderkamp A-C, Thuróczy C-E, Van Dijken GL, De Baar HJW, et al. 2012. Phytoplankton biomass and pigment responses to Fe amendments in the Pine Island and Amundsen polynyas. *Deep-Sea Res Pt II* **71–76**: 61–76.

Mills MM, Kropuenske LR, Van Dijken GL, Alderkamp A-C, Berg GM, et al. 2010. Photophysiology in two major Southern Ocean phytoplankton taxa: photosynthesis and growth of *Phaeocystis antarctica* (Prymnesiophyceae) and *Fragilariopsis cylindrus* (Bacillariophyceae) under simulated mixed layer irradiance. *J Phycol* **46**: 1114–1127.

Mitchell BG, Brody EA, Holm-Hansen O, McClain C, Bishop J. 1991. Light limitation of phytoplankton biomass and macronutrient utilization in the Southern Ocean. *Limnol Oceanogr* **36**: 1662–1677.

Mitchell BG, Kiefer DA. 1988. Chlorophyll-alpha specific absorption and fluorescence excitation-spectra for light-limited phytoplankton. *Deep-Sea Res Pt I* **35**: 639–663.

Moore CM, Suggett DJ, Hickmann AE, Kim Y-N, Tweddle JF, et al. 2006. Phytoplankton photoacclimation and photo-adaptation in response to environmental gradients in a shelf sea. *Limnol Oceanogr* **51**: 936–949.

Mu L, Stammerjohn SS, Lowry KE, Yager PY. 2014. Spatial variability of surface pCO_2 and air-sea CO_2 flux in the Amundsen Sea Polynya, Antarctica. *Elem Sci Anth* **2**: 000036. doi: 10.12952/journal.elementa.000036.

Planquette H, Sherrell RM. 2012.Sampling for particulate trace element determination using water sampling bottles: methodology and comparison to in situ pumps. *Limnol Oceanogr Methods* **10**: 367–388.

Platt T, Gallegos CL, Harrison WG. 1980. Photoinhibition of photosynthesis in natural assemblages of marine-phytoplankton. *J Mar Res* **38**: 687–701.

Pritchard HD, Arthern RJ, Vaughan DG, Edwards LA. 2009. Extensive dynamic thinning on the margins of the Greenland and Antarctic ice sheets. *Nature* **461**: 971–975.

Raiswell R. 2011. Iceberg-hosted nanoparticulate Fe in the Southern Ocean: Mineralogy, origin, dissolution kinetics and source of bioavailable Fe. *Deep-Sea Res Pt II* **58**: 1364–1375.

Raiswell R, Benning LG, Tranter M, Tulaczyk S. 2008. Bioavailable iron in the Southern Ocean: the significance of the iceberg conveyor belt. *Geochem Trans* **9**: 7. doi: 10.1186/1467-4866-9-7.

Raiswell R, Tranter M, Benning LG, Siegert M, De'ath R, et al. 2006. Contributions from glacially derived sediment to the global iron (oxyhydr)oxide cycle: Implications for iron delivery to the oceans. *Geochim Cosmochim Ac* **70**: 2765–2780.

Randall-Goodwin E, Meredith PM, Sherrell RM, Yager PL, Alderkamp AC, et al. 2015. Meltwater distributions in the Amundsen Sea Polynya, Antarctica. *Elem Sci Anth:* under review for the ASPIRE Special Feature.

Raven JA. 1990. Predictions of Mn and Fe use efficiencies of phototrophic growth as a function of light availability for growth and of C assimilation pathway. *New Phytol* **116**: 1–18.

Rignot E, Jacobs SS, Mouginot J, Scheuchi B. 2013. Ice-shelf melting around Antarctica, *Science* **341**: 266–270.

Rijkenberg MJA, Gerringa LJA, Carolus VE, Velzeboer I, De Baar HJW. 2006. Enhancement and inhibition of iron photoreduction by individual ligands in open ocean seawater. *Geochim Cosmochim Acta* **70**: 2790–2805.

Rijkenberg MJA, Gerringa LJA, Timmermans KR, Fischer AC, Kroon KJ, et al. 2008. Marine diatoms enhance the reactive iron pool by modification of iron-binding ligands and stimulation of iron-photoreduction. *Mar Chem* **109**: 29–44.

Riley GA. 1957. Phytoplankton of the North Central Sargasso Sea, 1950–52. *Limnol Oceanogr* **2**: 252–270.

Sarmiento JL, Slater R, Barber R, Bopp L, Doney SC, et al. 2004. Response of ocean ecosystems to climate warming. *Global Biogeochem Cy* **18**: GB3003. doi: 10.1029/2003GB002134.

Schoemann V, Wollast R, Chou L, Lancelot C. 2001. Effects of photosynthesison the accumulation of Mn and Fe by *Phaeocystis* colonies. *Limnol Oceanogr* **46**: 1065–1076.

Schofield O, Miles T, Alderkamp A-C, Lee SH, Haskins C, et al. 2015. *In situ* phytoplankton distributions in the Amundsen Sea Polynya measured by autonomous gliders. *Elem Sci Anth:* under review for the ASPIRE Special Feature.

Sedwick PN, DiTullio GR. 1997. Regulation of algal blooms in Antarctic shelf waters by the release of iron from melting sea ice. *Geophys Res Lett* **24**: 2515–2518.

Sedwick PN, DiTullio GR, Mackey DJ.2000. Iron and manganese in the Ross Sea, Antarctica: Seasonal iron limitation in Antarctic shelf waters. *J Geophys Res-Oceans* **105**: 11321–11336.

Sedwick PN, Marsay CM, Sohst BM, Aguilar-Islas AM, Lohan MC, et al. 2011. Early season depletion of dissolved iron in the Ross Sea polynya: Implications for iron dynamics on the Antarctic continental shelf. *J Geophys Res-Oceans* **116**: C12019. doi: 10.1029/2010JC006553.

Shaw TJ, Raiswell R, Hexel CR, Vu HP, Moore WS, et al. 2011. Input, composition, and potential impact of terrigenous material from free-drifting icebergs in the Weddell Sea. *Deep-Sea Res* **58**:1376–1383.

Sherrell RM, Lagerström M, Forsch K, Stammerjohn SE, Yager PL. 2015. Dynamics of dissolved iron and other bioactive trace metals (Mn, Ni, Cu, Zn) in the Amundsen Sea Polynya, Antarctica. *Elem Sci Anth:* under review for the ASPIRE Special Feature.

Smith WO, Barber DG, eds. 2007. *Polynyas: Windows to the World*. Amsterdam: Elsevier Science. (Elsevier Oceanography Series. Vol. 74). 474 pp.

Smith WO, Tozzi S, Long MC, Sedwick PN, Peloquin JA, et al. 2013. Spatial and temporal variations in variable fluorescence in the Ross Sea (Antarctica): Oceanographic correlates and bloom dynamics. *Deep-Sea Res Pt I* **79**: 141–155.

St-Laurent P, Klinck JM, Dinniman MS. 2013. On the role of coastal troughs in the circulation of warm Circumpolar Deep Water on Antarctic shelves. *J Phys Oceanogr* **43**: 51–64.

Strzepek RF, Harrison PJ. 2004. Photosynthetic architecture differs in coastal and oceanic diatoms. *Nature* **431**: 689–692.

Strzepek RF, Hunter KA, Frew RD, Harrison PJ, Boyd PW. 2012. Iron-light interactions differ in Southern Ocean phytoplankton. *Limnol Oceanogr* **57**: 1182–1200. doi: 10.4319/lo.2012.57.4.1182.

Strzepek RF, Price NM. 2000. Influence of irradiance and temperature on the iron content of the marine diatom *Thalassiosira weissflogii* (Bacillariophyceae). *Mar Ecol-Prog Ser* **206**: 107–117. doi: 10.3354/meps206107.

Suggett DJ, MacIntyre HL, Geider RJ. 2004. Evaluation of biophysical and optimal determinations of light absorption by photosystem II in phytoplankton. *Limnol Oceanogr Methods* **2**: 316–332.

Tagliabue A, Arrigo KR. 2005. Iron in the Ross Sea: 1. Impact on CO_2 fluxes via variation in phytoplankton functional group and non-Redfield stoichiometry. *J Geophys Res-Oceans* **110**: C03009. doi: 10.1029/2004JC002531.

Thoma M, Jenkins A, Holland D, Jacobs SS. 2008. Modelling Circumpolar Deep Water intrusions on the Amundsen Sea continental shelf, Antarctica. *Geophys Res Lett* **35**: 1–6. doi:10.1029/2008GL034939.

Thuróczy C-E, Alderkamp A-C, Laan P, Gerringa LJA, De Baar HJW, et al. 2012. Key role of organic complexation of iron in sustaining the phytoplankton blooms in the Pine Island and Amundsen Polynyas (Southern Ocean). *Deep-Sea Res Pt II* **71–76**: 49–60.

Twining BS, Baines SB. 2013. The trace metal composition of marine phytoplankton. *Ann Rev Mar Sci* **5**: 191–215.

Twining BS, Baines SB, Fisher NS, Landry MR. 2004. Cellular iron contents of plankton during the Southern Ocean Iron Experiment (SOFeX). *Deep-Sea Res Pt I* **51**: 1827–1850.

Van Hilst CM, Smith WO. 2002. Photosynthesis/irradiance relationships in the Ross Sea, Antarctica, and their control by phytoplankton assemblage composition and environmental factors. *Mar Ecol-Prog Ser* **226**: 1–12.

Van Leeuwe MA, Stefels J. 2007. Photosynthetic responses in *Phaeocystis antarctica* towards varying light and iron conditions. *Biogeochemistry* **83**: 61–70.

Vassiliev IR, Kolber Z, Wyman KD, Mauzerall D, Shukla VK, et al. 1995. Effects of iron limitation on photosystem-II composition and light utilization in *Dunaliella tertiolecta*. *Plant Physiol* **109**: 963–972.

Vernet M, Sines K, Chakos D, Ekern L. 2011. Impacts on phytoplankton dynamics by free-drifting icebergs in the NW Weddell Sea. *Deep-Sea Res Pt II* **58**: 1422–1435.

Visser F, Gerringa LJA, Van der Gaast SJ, De Baar HJW, Timmermans KR. 2003. The role of reactivity and iron content of aerosol dust on growth rates of two Antarctic diatom species. *J Phycol* **39**: 1085–1094.

Wåhlin AK, Kalén O, Arneborg L, Björk G, Carvajal GK, et al. 2013. Variability of warm deep water inflow in a submarine trough on the Amundsen Sea shelf. *J Phys Oceanogr* **43**: 2054–2070. doi: 10.1175/JPO-D-12-0157.1.

Webb WL, Newton M, Starr D. 1974. Carbon dioxide exchange of *Alnus rubra.* A mathematical model. *Oecologia* **17**: 281–291.

Williams CM, Dupont A, Post AF, Riemann L, Dinasquet J, et al. 2015. Pelagic microbial heterotrophy in response to a highly productive bloom of the marine haptophyte *Phaeocystis antarctica* in the Amundsen Sea Polynya. *Elem Sci Anth:* under review for the ASPIRE Special Feature.

Wright SW, Jeffrey S, Mantoura R, Lewellyn C, Bjornland C, et al.1991. An improved HPLC method for the analysis of chlorophylls and carotenoids from marine phytoplankton. *Mar Ecol-Prog Ser* **77**: 183–196.

Wright SW, Thomas DP, Marchant HJ, Higgins HW, Mackey MD, et al. 1996. Analysis of phytoplankton of the Australian sector of the Southern Ocean: Comparisons of microscopy and size frequency data with interpretations of pigment HPLC data using the 'CHEMTAX' matrix factorisation program. *Mar Ecol-Prog Ser* **144**: 285–298.

Wright SW, Van den Enden RL, Pearce I, Davidson AT, Scott FJ, et al. 2010. Phytoplankton community structure and stocks in the Southern Ocean (30–80° E) determined by CHEMTAX analysis of HPLC pigment signatures. *Deep-Sea Res Pt I* **57**: 758–778.

Yager PL, Sherrell RM, Alderkamp AC, Ingall ED, Ducklow HW. 2014. Net community production and export in the Amundsen Sea Polynya (western Antarctica); with comparisons to Arctic polynyas and a link to climate sensitivity. 2014. *Ocean Sciences meeting*. Honolulu, Hawaii.

Yager PL, Sherrell RM, Stammerjohn SE, Alderkamp A-C, Schofield O, et al. 2012. ASPIRE: The Amundsen Sea Polynya International Research Expedition. *Oceanography* **25**: 40–53. doi: 10.5670/oceanog.2012.73.

Zapata M, Jeffrey SW, Wright SW, Rodriguez F, Garrido JL, et al. 2004. Photosynthetic pigments in 37 species (65 strains) of Haptophyta: implications for oceanography and chemotaxonomy. *Mar Ecol-Prog Ser* **270**: 83–102.

Contributions

- Substantial contributions to conception and design: ACA, GLD, PLY, KRA
- Acquisition of data: ACA, GLD, KEL, TLC, ML, RMS, CH, ER, SES
- Analysis and interpretation of data: ACA, GLD, KEL, TLC, RMS, OS, SES, PLY, KRA
- Drafting the article or revising it critically for important intellectual content: all Authors
- Final approval of the version to be published: all Authors

Acknowledgments

We thank the captain, crew, technicians, and cruise participants of the NBP 10-05 ASPIRE cruise for their help and Jennifer Vreeland for HPLC analysis. Loes Gerringa and two anonymous reviewers are acknowledged for helpful comments on an earlier version. ASPIRE was part of "Oden Southern Ocean" (SWDARP 2010/11) organized by the Swedish Polar Research Secretariat and National Science Foundation Office of Polar Programs.

Funding information

This research was supported by the National Science Foundation Office of Polar Programs, Antarctic Organisms (ANT-0944727 to KRA, ANT-0839069 to PY, ANT-0838995 to RMS and OS, and ANT-0838975 to SS).

Competing interests

Authors declare that there are no competing interests.

Data accessibility statement

Data are available in the BCO-DMO database: http://www.bco-dmo.org/dataset/546372.